J. Fluid Mech., page 1 of 30
doi:10.1017/S0022112011000486

Ellipsoidal capsules in simple shear flow: prolate versus oblate initial shapes

J. WALTER, A.-V. SALSAC AND D. BARTHÈS-BIESEL†
Laboratoire Biomécanique et Bioingénierie (UMR CNRS 6600),
Université de Technologie de Compiègne, BP 20529, 60205 Compiègne, France

(Received 6 July 2010; revised 21 December 2010; accepted 25 January 2011)

The large deformations of an initially-ellipsoidal capsule in a simple shear flow are studied by coupling a boundary integral method for the internal and external flows and a finite-element method for the capsule wall motion. Oblate and prolate spheroids are considered (initial aspect ratios: 0.5 and 2) in the case where the internal and external fluids have the same viscosity and the revolution axis of the initial spheroid lies in the shear plane. The influence of the membrane mechanical properties (mechanical law and ratio of shear to area dilatation moduli) on the capsule behaviour is investigated. Two regimes are found depending on the value of a capillary number comparing viscous and elastic forces. At low capillary numbers, the capsule tumbles, behaving mostly like a solid particle. At higher capillary numbers, the capsule has a fluid-like behaviour and oscillates in the shear flow while its membrane continuously rotates around its deformed shape. During the tumbling-to-swinging transition, the capsule transits through an almost circular profile in the shear plane for which a long axis can no longer be defined. The critical transition capillary number is found to depend mainly on the initial shape of the capsule and on its shear modulus, and weakly on the area dilatation modulus. Qualitatively, oblate and prolate capsules are found to behave similarly, particularly at large capillary numbers when the influence of the initial state fades out. However, the capillary number at which the transition occurs is significantly lower for oblate spheroids.

Key words: capsule/cell dynamics

1. Introduction

A microcapsule is a small liquid droplet enclosed in a thin hyperelastic membrane. Artificial capsules have numerous applications in cosmetics, drug vectorization and cell encapsulation. Cells (particularly red blood cells, which do not have a nucleus) can also be modelled mechanically as capsules.

When placed in a simple shear flow, an initially-spherical capsule elongates in the straining direction of the flow; provided that the flow strength remains moderate, a steady state can be reached. Due to the vorticity of the flow, the membrane of the capsule rotates around the deformed shape, in a *tank-treading* motion. This behaviour was analysed theoretically in the small deformation limit by Barthès-Biesel & Rallison (1981) and later reproduced numerically for large deformations (e.g. Ramanujan & Pozrikidis 1998; Lac *et al.* 2004; Doddi & Bagchi 2008; Li &

† Email address for correspondence: dbb@utc.fr

Sarkar 2008). However, the experimental work of Chang & Olbricht (1993) and Walter, Rehage & Leonhard (2001) showed a more complex behaviour of the capsule: the deformation and inclination of the capsule shape were found to undergo small oscillations, with a periodicity determined by the tank-treading period and thus the shear rate. This phenomenon, which shall be referred to as *swinging* in this article, can be interpreted by considering that the capsules had slightly-non-spherical reference shapes (Walter *et al.* report aspect ratios of approximately 0.97). Thus, the successive states of the capsule as the membrane tank-treads are not completely equivalent and the deformation and inclination can vary over time. Ramanujan & Pozrikidis (1998) studied the motion of oblate spheroids in a simple shear flow numerically and found that they indeed exhibited swinging, while spherical capsules did not. Since even a slight deviation from sphericity in experimental capsules leads to a noticeable swinging phenomenon, it appears that numerical models need to take into account these effects, even for quasi-spherical capsules. Furthermore, recent advances in encapsulation in microfluidic channels (e.g. Xiang *et al.* 2008; Liu *et al.* 2009) are paving the way for the production of highly-non-spherical capsules with arbitrary aspect ratios, whether oblate or prolate. Such artificial capsules have a higher surface-area-to-volume ratio than spherical ones and may therefore have interesting transport and diffusion applications.

Another reason for studying non-spherical capsules is understanding the motion of red blood cells. It has long been known that red blood cells placed in a Couette flow exhibit a solid-like *tumbling* motion at low shear rates and a tank-treading motion at high shear rates (Schmid-Schönbein & Wells 1969; Goldsmith & Marlow 1972). However, the recent experimental work of Abkarian, Faivre & Viallat (2007) showed that swinging is noticeable at intermediate shear rates. This means that the wall of a red blood cell can behave similarly to an elastic membrane having a non-spherical reference shape. Such a behaviour is likely to be induced by the protein cytoskeleton that lines the intracellular side of the cell wall. Abkarian *et al.* also reported that the tumbling-to-swinging transition occurred through an *intermittent regime*, during which the cell alternates between tumbling and swinging. These findings have led to a renewed interest in non-spherical capsules, with several theoretical and numerical articles published on the subject in recent years.

Skotheim & Secomb (2007), extending the analysis of Keller & Skalak (1982), developed a simplified analytical model in order to predict the regime of deformation of a capsule as a function of two parameters: the ratio of the viscosities of the internal and external fluids and a capillary number, which compares the work of the fluid shear forces to the elastic energy stored in the membrane. This model is based on the strong hypothesis that the three-dimensional shape of the capsule remains unchanged over time. It postulates that the capsule behaviour is dominated by the competition between two energies: the energy provided by the viscous flows, which causes the tank-treading motion of the wall, and the strain energy of the membrane, which tends to restore the original configuration. The equations of this model lead to the tumbling and swinging regimes, as well as the intermittent behaviour at the transition. For a given fixed shape of the capsule, a phase diagram can be constructed distinguishing the motion modes as a function of the two non-dimensional parameters. The model also provides values for the amplitude and the mean value of the oscillations of the inclination. In a recent article, Finken, Kessler & Seifert (2010) conducted a more general study by performing a systematic expansion of the equations of motion for the small deformation of a quasi-spherical capsule. They found that, contrary to the

assumption of Skotheim & Secomb (2007), the deformation of the capsule shape plays a large part in its dynamics.

The first three-dimensional numerical study of non-spherical capsules was the work of Ramanujan & Pozrikidis (1998) referred to above. Because of computing limitations, this study was limited to a few particular cases, mostly for capsules with an aspect ratio of 0.9, and did not investigate very low flow rates: it therefore did not find the tumbling regime. Sui *et al.* (2008) studied oblate spheroidal capsules with identical viscosities for the internal and external fluids and modelled the membrane behaviour with the neo-Hookean law. They found both the tumbling and swinging regimes, and explored some values of the parameters governing the two regimes and their transition, showing that the oscillation of the capsule deformation was maximum at the transition. In the swinging regime, the oscillations were found to decrease as the flow strength was increased. Le & Tan (2010) also studied oblate spheroidal capsules, with various values of the aspect ratio and viscosity ratio. Large amounts of wrinkling were found to occur at low shear rates, rendering the computations unstable. These authors also briefly investigated the behaviour of capsule with a biconcave reference shape in the tumbling regime.

Two systematic studies were conducted in order to draw up phase diagrams that could be compared with the theory of Skotheim & Secomb (2007). Kessler, Finken & Seifert (2008) studied oblate spheroids that were only slightly non-spherical (aspect ratio of 0.9). They considered moderate deformation and modelled the capsule wall using Hooke's law, to which they added a small bending stiffness. They showed that, even if the analytical model of Skotheim & Secomb provides an insight into the physical phenomena governing the capsule deformation, it does not fully account for the behaviour of the capsule. In particular, the shape of the capsule does not remain constant during motion as well as when the parameters vary. We are, however, surprised by some of the results obtained by Kessler *et al.* (2008) in that study. The authors validated their numerical model by providing results on the deformation of a very viscous spherical capsule with a viscosity contrast $\lambda = 10$ between the internal and external phases. The steady state deformation values are larger than those found by earlier numerical models for $\lambda = 5$ (Ramanujan & Pozrikidis 1998; Doddi & Bagchi 2008) or those predicted by the asymptotic theory for highly viscous capsules (Barthès-Biesel & Rallison 1981). Furthermore Kessler *et al.* (2008) used a bending modulus which is very large compared to the surface shear modulus. Indeed, if one assumes that the membrane is a 3D sheet of isotropic material, the value of the bending modulus corresponds to a membrane thickness that is 17 % of the capsule radius (the detailed computation is developed in the Discussion section). Such a large thickness is expected to create correspondingly large bending effects that limit the deformation even further. Being interested in capsules with aspect ratios quite different from unity (1.5 and 0.5) and with a membrane dominated by in-plane elasticity rather than bending, we do not expect to be able to use the results of Kessler *et al.* for quantitative comparisons.

Recently, Bagchi & Kalluri (2009) also constructed phase diagrams for oblate spheroids (aspect ratios 0.7 and 0.9) with membranes described by the hyperelastic law proposed by Skalak *et al.* (1973). They studied the so-called *vacillating–breathing* regime, which is similar to the swinging regime but with much larger amplitudes of the oscillations. It is noteworthy that none of the five numerical studies cited above were able to reproduce the intermittent regime described by Abkarian *et al.* (2007).

The aim of the present study is to compare the behaviour of prolate and oblate spheroidal capsules in a simple shear flow. This work appears to be the first numerical

study on the behaviour of prolate spheroidal capsules. Particular attention will be paid to the various regimes observed and to the transition between them, with the intent of confronting the physical understanding of these motion modes with the results of the computations. A systematic study of the influence of the properties of the capsule wall (material law and ratio of the area dilatation modulus to the shear modulus) will be conducted. However, the influence of the viscosity ratio will not be studied; the internal and external fluids will be assumed to have the same viscosity throughout the study.

In §§ 2 and 3, we introduce the problem at stake, the numerical method as well as the notations adapted to the study of ellipsoidal capsules. We then present in § 4 the characteristics of the tumbling and swinging regimes, and investigate the transition between them. The results of a full parametric study are presented in § 5, in which we consider the influence of the capillary number on the motion for two membrane laws and two aspect ratios. The Poisson ratio is then varied in § 6 and its influence on the swinging regime and on the tumbling-to-swinging transition is investigated. Finally, a discussion of the key phenomena governing the dynamics of ellipsoidal capsules is conducted in § 7.

2. Problem description

The motion of a capsule in flow can now be considered as a classical problem, which is only briefly outlined here (for more details, see Pozrikidis 1992; Barthès-Biesel 2003).

2.1. *Hydrodynamics*

Consider a capsule of typical dimension ℓ, filled with an incompressible liquid and enclosed by an infinitely thin membrane of surface shear elastic modulus G_s and area dilatation modulus K_s. The capsule is freely suspended in another incompressible liquid undergoing a simple shear flow with shear rate $\dot{\gamma}$. The external and internal liquids are Newtonian with equal viscosity μ and density ρ. Gravitational effects are thus neglected as the capsule is neutrally buoyant. The Reynolds number of the flow based on the capsule dimension, $Re = \rho\dot{\gamma}\ell^2/\mu$, is assumed to be very small, so that the motion of the internal and external liquids is governed by the Stokes equations. In the laboratory Cartesian frame of reference $(\boldsymbol{e}_1, \boldsymbol{e}_2, \boldsymbol{e}_3)$ centred at the capsule centre of mass, the interfacial velocity can be written in terms of an integral equation over the instantaneous deformed capsule surface S (Pozrikidis 1992)

$$\boldsymbol{v}(\boldsymbol{x}) = \boldsymbol{v}^{\infty}(\boldsymbol{x}) - \frac{1}{8\pi\mu}\int_S \boldsymbol{G}(\boldsymbol{x}, \boldsymbol{y}) \cdot [\boldsymbol{\sigma}(\boldsymbol{y})] \cdot \boldsymbol{n}(\boldsymbol{y})\, \mathrm{d}S(\boldsymbol{y})\,, \tag{2.1}$$

where $[\boldsymbol{\sigma}]$ is the stress tensor jump across the interface, $\boldsymbol{n}$ is the outward unit normal vector to S and $\boldsymbol{v}^{\infty}$ is the undisturbed flow velocity. The Oseen tensor $\boldsymbol{G}$ is defined as

$$\boldsymbol{G}(\boldsymbol{x}, \boldsymbol{y}) = \frac{1}{r}\boldsymbol{I} + \frac{1}{r^3}\boldsymbol{r} \otimes \boldsymbol{r}\,, \tag{2.2}$$

where $\boldsymbol{r} = \boldsymbol{x} - \boldsymbol{y}$, $r = \|\boldsymbol{r}\|$ and $\boldsymbol{I}$ is the identity tensor. This formulation ensures that the velocity disturbance vanishes far from the capsule. Two fluid–structure coupling conditions are next introduced:

(i) The kinematic condition requires continuity of the membrane velocity and of the interfacial fluid velocity

$$\boldsymbol{v}(\boldsymbol{x}, t) = \frac{\partial \boldsymbol{x}(\boldsymbol{X}, t)}{\partial t}, \quad \boldsymbol{x} \in S\,. \tag{2.3}$$

The vector $\boldsymbol{x}$ is the current position of a membrane material point, which is located at $\boldsymbol{X}$ in the reference state.

(ii) The dynamic condition requires that the load $\boldsymbol{q}$ exerted on the membrane be equal to the viscous traction's jump across the interface

$$[\boldsymbol{\sigma}(\boldsymbol{x})] \cdot \boldsymbol{n} = \boldsymbol{q}. \tag{2.4}$$

An important parameter of the problem is the ratio of viscous and elastic forces expressed by the dimensionless group

$$Ca = \frac{\mu \dot{\gamma} \ell}{G_s}, \tag{2.5}$$

that plays the role of a capillary number, where surface tension is replaced by the membrane shear elastic modulus. For a given capsule, Ca may also be viewed as a non-dimensional shear rate.

2.2. *Membrane mechanics*

When the thickness of a capsule membrane is small compared to the capsule dimensions and typical radius of curvature, the membrane can be modelled as a hyperelastic *surface* devoid of bending resistance (e.g. Skalak *et al.* 1973). Even with this simplification, quantifying the capsule deformation is a complicated geometrical problem involving the description of curved surfaces and their deformation. We will briefly outline the basic necessary concepts.

A membrane material point, identified by its position $\boldsymbol{X}$ in the reference state, is displaced to the position $\boldsymbol{x}(\boldsymbol{X}, t)$ in the deformed state. By convention, all quantities in the reference state are denoted by capital letters. Because the bending stiffness is neglected, deformation occurs only in the plane of the membrane and the normal vector to the surface remains normal during deformation. The gradient of the transformation $\boldsymbol{F}$ is defined as

$$\mathrm{d}\boldsymbol{x} = \boldsymbol{F} \cdot \mathrm{d}\boldsymbol{X}. \tag{2.6}$$

The local deformation of the surface can be measured by the Green–Lagrange strain tensor

$$\boldsymbol{e} = \tfrac{1}{2}(\boldsymbol{F}^{\mathrm{T}} \cdot \boldsymbol{F} - \boldsymbol{I}). \tag{2.7}$$

The membrane deformation can also be quantified by the principal dilatation ratios λ_1 and λ_2 in its plane. Two deformation invariants are generally used:

$$I_1 = \lambda_1^2 + \lambda_2^2 - 2, \quad I_2 = \lambda_1^2 \lambda_2^2 - 1 = J_s^2 - 1. \tag{2.8}$$

The Jacobian $J_s = \lambda_1 \lambda_2$ represents the ratio of the deformed to the undeformed surface areas.

Elastic stresses in an infinitely thin membrane are replaced by elastic tensions corresponding to forces per unit arclength measured in the plane of the membrane. When the membrane is a two-dimensional isotropic material, the Cauchy tension tensor $\boldsymbol{\tau}$ can be related to a strain energy function per unit area of undeformed membrane $w_s(I_1, I_2)$ by

$$\boldsymbol{\tau} = \frac{1}{J_s} \boldsymbol{F} \cdot \frac{\partial w_s}{\partial \boldsymbol{e}} \cdot \boldsymbol{F}^{\mathrm{T}}. \tag{2.9}$$

A number of laws are available to model thin hyperelastic membranes (Oden 1972). Different material behaviours can be described for a large deformation, including the strain-softening behaviour of gelled membranes exhibiting rubber-like elasticity or the strain-hardening behaviour of membranes made of a polymerized network with strong

covalent links. Only simple laws with constant material coefficients are considered in this analysis. In the limit of small deformation, all laws reduce to the two-dimensional Hooke law with surface shear elastic modulus G_s and surface Poisson ratio ν_s ($\nu_s \in]-1, +1[$). The area dilatation modulus is then $K_s = G_s(1+\nu_s)/(1-\nu_s)$ and an area-incompressible membrane corresponds to $\nu_s = 1$.

The widely used neo-Hookean law (NH) describes the behaviour of an infinitely thin sheet of a three-dimensional isotropic and incompressible material

$$w_s^{NH} = \frac{G_s^{NH}}{2}\left(I_1 - 1 + \frac{1}{I_2+1}\right). \tag{2.10}$$

Because of volume incompressibility, area dilatation is balanced by membrane thinning, and the area dilatation modulus is $K_s^{NH} = 3G_s^{NH}$. Another law (Sk) has been derived by Skalak *et al.* (1973) for two-dimensional materials with independent surface shear and area dilatation moduli

$$w_s^{Sk} = \frac{G_s^{Sk}}{4}\left(I_1^2 + 2I_1 - 2I_2 + CI_2^2\right), \quad C > -1/2. \tag{2.11}$$

The area dilatation modulus is $K_s^{Sk} = G_s^{Sk}(1+2C)$. The Sk law was initially designed to model the area-incompressible membrane of biological cells, such as red blood cells, corresponding to $C \gg 1$. However, the law is very general and can be used to also model other types of membranes, for which the shear and area dilatation moduli are of the same order of magnitude, as in the case of albumin–alginate membranes (Carin *et al.* 2003).

Equivalence between the laws arises when

$$G_s = G_s^{NH}, \quad \nu_s = 1/2, \quad \text{for NH law,} \tag{2.12}$$

and

$$G_s = G_s^{Sk}, \quad \nu_s = \frac{C}{1+C}, \quad \text{for Sk law.} \tag{2.13}$$

When $C = 1$, the NH and Sk laws predict the same small deformation behaviour of a membrane with $K_s = 3G_s$, corresponding to $\nu_s = 1/2$. However, different nonlinear tension–strain relations are obtained under a large deformation. In particular, it can be easily checked that the NH law is strain-softening under uniaxial stretching, whereas the Sk law is strain-hardening (Barthès-Biesel, Diaz & Dhenin 2002).

Because of the negligible inertia of a membrane with small thickness, the membrane motion is governed by the local equilibrium equation

$$\nabla_s \cdot \boldsymbol{\tau} + \boldsymbol{q} = \boldsymbol{0}, \tag{2.14}$$

where $\boldsymbol{q}$ is the external load exerted by the fluids and $\nabla_s\cdot$ is the surface divergence operator in the deformed configuration. Equation (2.14) can also be written in a weak form using the virtual work principle: for any virtual displacement field $\hat{\boldsymbol{u}}$, balancing the internal and external virtual work requires

$$\int_S \hat{\boldsymbol{u}} \cdot \boldsymbol{q}\, \mathrm{d}S - \int_S \hat{\boldsymbol{\varepsilon}}(\hat{\boldsymbol{u}}) : \boldsymbol{\tau}\, \mathrm{d}S = 0, \tag{2.15}$$

where $\hat{\boldsymbol{\varepsilon}}(\hat{\boldsymbol{u}}) = \frac{1}{2}(\nabla_s \hat{\boldsymbol{u}} + \nabla_s \hat{\boldsymbol{u}}^{\mathrm{T}})$ is the virtual strain tensor.

Since the bending modulus of the membrane has been neglected, the capsule wall should be under tension everywhere; otherwise it may buckle locally in the regions where the elastic tensions are compressive. This phenomenon is well known for thin

elastic sheets, see for example Cerda & Mahadevan (2003) and Luo & Pozrikidis (2007). In that case, a full shell model including bending moments and transverse shear forces would be necessary to describe properly the mechanics of the capsule wall.

2.3. *Motion of an ellipsoidal capsule in a simple shear flow*

We consider a capsule that is initially spheroidal in its reference undeformed state, with semi-axes along the revolution axis and the orthogonal directions denoted a and b, respectively. If $a/b < 1$, the spheroid is oblate and if $a/b > 1$, it is prolate. We choose as length scale ℓ the radius of the sphere, which has the same volume as the ellipsoid

$$\ell = \sqrt[3]{ab^2} = a(b/a)^{2/3}. \tag{2.16}$$

The capsule is freely suspended in a simple shear flow in the (x_1, x_2) plane

$$\boldsymbol{v}^{\infty} = \dot{\gamma} x_2 \, \boldsymbol{e}_1. \tag{2.17}$$

When the initial shape of the capsule is spherical, all the material points are equivalent and the capsule takes a *steady* deformed profile around which the membrane rotates because of the flow vorticity (*tank-treading motion*). However, when the reference shape is ellipsoidal, the membrane points are not equivalent. Consequently, a stationary steady state is not possible and a periodic motion of the deformed capsule must occur. To simplify the situation, we consider a capsule with its revolution axis along $\boldsymbol{e}_2$ at time $t = 0$. Thus, the initial profile equation is given by

$$\left(\frac{X_1}{b}\right)^2 + \left(\frac{X_2}{a}\right)^2 + \left(\frac{X_3}{b}\right)^2 = 1. \tag{2.18}$$

Since the capsule profile may be quite difficult to characterize, we evaluate the capsule distortion by the deformation of its ellipsoid of inertia (Ramanujan & Pozrikidis 1998). This method is widely used, but gives approximate results when the deformed particle shape is far from ellipsoidal. By symmetry, the material points initially located in the shear plane (x_1, x_2) remain in it and two of the principal axes of the ellipsoid of inertia with semi-axes L_1 and L_2 ($L_1 \geqslant L_2$) are also located in the shear plane. Correspondingly, it is convenient to quantify the three-dimensional capsule deformation with the deformation of the intersection of the profile with the shear plane. The Taylor deformation parameter is then defined as

$$D_{12} = \frac{L_1 - L_2}{L_1 + L_2}. \tag{2.19}$$

Note that, contrary to a spherical capsule, the initial value of D_{12} is not zero and is given by $D_{12}^0 = |a - b|/(a + b)$.

The motion of a capsule is quite complex as it continuously undergoes deformation and orientation change over time, while the membrane rotates around it. To decompose and evaluate these two motion components, we adopt the notations of Kessler *et al.* (2008) and follow in time the position of a material point P in the shear plane. As shown in figure 1, the angle between OP and $\boldsymbol{e}_1$ is denoted $\alpha(t)$, while the angle between the ellipsoid long axis (L_1) and $\boldsymbol{e}_1$ is denoted $\beta(t)$. The difference $\delta(t) = \alpha(t) - \beta(t) - [\alpha(0) - \beta(0)]$ measures the angular displacement of P with respect to its initial position in the ellipsoid principal axes. By definition, $\delta(0) = 0$. We consider the values of $\beta(t)$ and $\delta(t)$ modulo 2π and arbitrarily limit their respective variations to the interval $[-\pi, \pi]$.

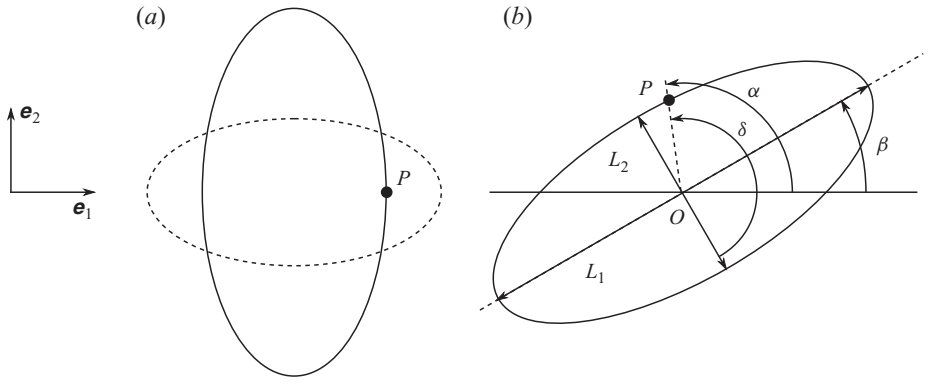

FIGURE 1. Representation in the shear plane ($\boldsymbol{e}_1, \boldsymbol{e}_2$) of ($a$) the initial state for prolate ($a/b = 2$, full line) and oblate ($a/b = 0.5$, dashed line) ellipsoidal capsules of equal volume and of (b) the ellipsoid of inertia of the deformed capsule with principal semi-axes L_1 and L_2 in the shear plane. The angle β gives the inclination of the deformed capsule; α shows the instantaneous position of the membrane material point P and $\delta(t)$ the position of P with respect to the ellipsoid principal axes.

When a periodic steady state is reached, we measure the period T of the capsule motion as the period of $\alpha(t)$. For the various quantities of the problem, we compute their mean value (denoted with an over line, e.g. $\bar{\beta}$) and their peak-to-peak amplitude (denoted by brackets, e.g. $[\beta]$) over one period.

3. Numerical method

The objective is to compute the motion and deformation of the capsule under the hydrodynamic stress until a periodic state is reached.

At time $t = 0$, the undeformed capsule is positioned in the external fluid (see § 2.3) and the flow is started. At any given time t, the position $\boldsymbol{x}(\boldsymbol{X}, t)$ of a membrane material point is known. The deformation of the capsule membrane may therefore be computed from (2.7) by comparison with the initial reference state. The elastic tensions $\boldsymbol{\tau}$ follow from (2.9), where the strain energy function w_s is given by the membrane constitutive law. The variational form (2.15) of the membrane equilibrium equation is solved by means of a finite-element method. It provides the values of the load $\boldsymbol{q}$ and thus of the traction jump $[\boldsymbol{\sigma}]\cdot\boldsymbol{n}$ on the membrane. The velocity $\boldsymbol{v}(\boldsymbol{x})$ of the membrane points is then computed explicitly from (2.1) using the boundary integral method. Finally, time integration of the kinematic condition (2.3) leads to the new position of the membrane material points and the process is repeated.

This algorithm is implemented by coupling the boundary integral method that solves for the internal and external flows with a membrane finite-element method that solves for the deformation of the capsule wall. This method, introduced by Walter *et al.* (2010) for initially-spherical capsules, was shown to be particularly efficient to deal with cases where the membrane is undergoing compression. In this case, discretizing the local equilibrium equation (2.14) requires the use of C^2-continuous functions, such as cubic B-splines (Lac *et al.* 2004). When the membrane grid points are squeezed together by compression, the polynomial tends to oscillate a lot, rendering the numerical scheme eventually unstable. Solving the membrane equilibrium equation (2.15) instead provides a better numerical stability, as the equation is integrated over

the surface. It was indeed shown that the method of Walter *et al.* (2010) was very stable in the presence of in-plane compression.

In the following, we briefly explain the coupling algorithm steps; more details may be found in the article by Walter *et al.* (2010) or in the book chapter by Barthès-Biesel, Walter & Salsac (2010).

3.1. *Mesh generation*

One of the main advantages of the boundary integral method besides its accuracy, is the need to only mesh the capsule wall surface. Moreover, a single mesh can be used to discretize all the unknowns of the problem: the position $\boldsymbol{x}$, the velocity $\boldsymbol{v}$, the load $\boldsymbol{q}$ and the virtual displacement $\hat{\boldsymbol{u}}$. The capsule wall is meshed using curved, triangular P_2 elements with six nodes (Cook *et al.* 2001), based on a quadratic interpolation of the unknowns within each element, which provides continuity from one element to the next, but discontinuous derivatives.

The initial mesh is constructed by first inscribing an icosahedron (regular polyhedron with 20 triangular faces) in a sphere. A new node is placed at the middle of each edge, so that each element is divided into four new elements; the new node is projected onto the sphere. The procedure is repeated until the desired number of elements is reached. To construct the P_2 elements, the edges are cut in half one last time and the nodes are projected onto the sphere (Ramanujan & Pozrikidis 1998). Finally, the mesh undergoes a linear transformation in one direction to create a spheroid with the desired aspect ratio.

3.2. *Finite-element procedure*

For a given instantaneous deformed shape, we define a finite-element space $\mathscr{V}_h$ corresponding to the mesh described above. The discretized solid problem consists of finding $\boldsymbol{q} \in \mathscr{V}_h$, such that the virtual work principle (2.15) is satisfied, i.e. $\forall \hat{\boldsymbol{u}} \in \mathscr{V}_h$. We are going to show that it can be written as a system of linear equations involving the values of $\boldsymbol{q}$ and $\hat{\boldsymbol{u}}$ at the nodes of the mesh, denoted respectively $\{q\}$ and $\{\hat{u}\}$.

Considering (2.15), one can see that the left-hand side depends linearly on $\boldsymbol{q}$ and $\hat{\boldsymbol{u}}$, and therefore on their nodal values; it can be written element-wise as

$$\int_S \hat{\boldsymbol{u}} \cdot \boldsymbol{q} \, \mathrm{d}S = \sum_{el} \{\hat{\boldsymbol{u}}_{el}\}^{\mathrm{T}} [\boldsymbol{M}_{el}] \{\boldsymbol{q}_{el}\}, \tag{3.1}$$

where the vectors $\{\boldsymbol{q}_{el}\}$ and $\{\hat{\boldsymbol{u}}_{el}\}$ hold the values of the load and the virtual displacement at the nodes of each element and the matrix $[\boldsymbol{M}_{el}]$ depends only on the metric properties of the element. In the next step, the elementary vectors and matrices are assembled into their global counterparts $\{q\}$, $\{\hat{u}\}$ and $[\boldsymbol{M}]$ (see e.g. Cook *et al.* 2001). We thus obtain

$$\int_S \hat{\boldsymbol{u}} \cdot \boldsymbol{q} \, \mathrm{d}S = \{\hat{u}\}^{\mathrm{T}} [\boldsymbol{M}] \{q\}, \tag{3.2}$$

the matrix $[\boldsymbol{M}]$ being a sparse matrix. Likewise, the right-hand side of (2.15) depends linearly on $\hat{\boldsymbol{u}}$ and its nodal components; it can thus be written as

$$\int_S \hat{\boldsymbol{\varepsilon}}(\hat{\boldsymbol{u}}) : \boldsymbol{\tau} \, \mathrm{d}S = \sum_{el} \{\hat{\boldsymbol{u}}_{el}\}^{\mathrm{T}} \{\boldsymbol{R}_{el}\}. \tag{3.3}$$

One can note that the vector $\{\boldsymbol{R}_{el}\}$ depends nonlinearly on the current deformation, as it contains the tensions $\boldsymbol{\tau}$. After assemblage, the right-hand side becomes

$$\int_S \hat{\boldsymbol{\varepsilon}}(\hat{\boldsymbol{u}}) : \boldsymbol{\tau}\, \mathrm{d}S = \{\hat{u}\}^{\mathrm{T}}\{R\}. \tag{3.4}$$

Details on the construction of $[\boldsymbol{M}]$ and $\{R\}$ are given in the article by Walter *et al.* (2010).

The discretized solid problem therefore becomes a linear system, from which the test function $\{\hat{u}\}$ can be eliminated, yielding

$$[\boldsymbol{M}]\{q\} = \{R\}. \tag{3.5}$$

In order to solve the solid problem, $[\boldsymbol{M}]$ and $\{R\}$ are first computed; surface integration is performed using six integration points on each element (Hammer, Marlowe & Stroud 1956). Equation (3.5) is then solved using the sparse solver PARDISO (Schenk & Gärtner 2004, 2006), yielding the load $\boldsymbol{q}$ on the capsule wall.

3.3. *Boundary integrals*

Once the load $\boldsymbol{q}$ is known, the velocity $\boldsymbol{v}$ at the points of the membrane can be obtained explicitly from (2.1). The equation is discretized on the same mesh as the solid problem. Twelve integration points are used on each element. Note that, when the integration point $\boldsymbol{y}$ approaches the node point $\boldsymbol{x}$, the kernel $\boldsymbol{G}$ becomes singular. Even if, numerically, the integration points do not coincide with the nodes, the distance r between them can become small enough to generate large numerical errors.

When $\boldsymbol{x}$ and $\boldsymbol{y}$ belong to the same element, we switch to polar coordinates centred on $\boldsymbol{x}$. This introduces a Jacobian, which goes to 0 as fast as r and eliminates the singularity in $\boldsymbol{G}$. In this case, six Gauss points are used for integration along each of the polar coordinates.

3.4. *Stability and convergence*

For all the following computations, we use a mesh with $N_E = 1280$ curved P_2 elements, corresponding to $N_N = 2562$ nodes. The numerical method was shown to be conditionally stable when the time step satisfies the condition

$$\dot{\gamma}\,\Delta t < O(hCa), \tag{3.6}$$

where h is the typical non-dimensional mesh size (Walter *et al.* 2010). For $Ca \geqslant 0.5$, we use $\dot{\gamma}\,\Delta t = 5 \times 10^{-3}$, and decrease the time step proportionally with Ca for lower values. When using Skalak's law for $C > 1$, we find that the stability condition becomes $\dot{\gamma}\,\Delta t < O(hCa/C)$; the time step is then modified accordingly. As shown by Walter *et al.* (2010), the convergence error obtained with these values of the mesh and time step is lower than 0.1 %.

It turns out that in many cases, part of the membrane undergoes compression. However, the numerical method introduces a membrane stiffness that contributes to the stability of the problem. It allows the numerical procedure to remain stable when in-plane compression and high curvatures may render other methods (e.g. B-spline projection) unstable. While it stabilizes the numerical procedure, the stiffness introduced is a byproduct of the numerical method: it, therefore, cannot be controlled or used to model the physical bending resistance of a capsule.

3.5. *Elastic energy*

In order to analyse the computational results, we propose to look at the elastic energy stored in the capsule wall. An energy E_m corresponding to the in-plane stresses can

be directly computed from the Lagrangian strain energy w_s for a given deformed state S as

$$E_m(S) = \int_{S_0} w_s(\boldsymbol{X}, t)\, \mathrm{d}S_0. \tag{3.7}$$

When the membrane behaviour follows Skalak's law, it is interesting to divide E_m into two parts: the first part E_m^G corresponds to shear strain effects and the second part E_m^K to areal dilatation effects. Separating both effects is particularly useful to study the influence of the parameter $C = K_s/2G_s - 1/2$. The two terms can be expressed as

$$E_m^G = \int_{S_0} \frac{G_s}{4}\left(I_1^2 + 2I_1 - 2I_2 - \frac{I_2^2}{2}\right) \mathrm{d}S_0\,, \quad E_m^K = \int_{S_0} 2K_s I_2^2\, \mathrm{d}S_0. \tag{3.8}$$

Note that, with this expression, the strain component of the membrane energy E_m^G may take negative values; the total energy E_m, however, always remains positive.

Even though the membrane model does not incorporate a bending stiffness, we are at times interested in estimating the importance of the wrinkling phenomenon, which occurs due to in-plane compression. We thus compute an approximate curvature energy E_b

$$E_b = \int_S \frac{\kappa}{2}(2H)^2\, \mathrm{d}S\,, \tag{3.9}$$

where κ is the bending modulus and H is the mean curvature (Helfrich 1973). As this definition of E_b implies a linear mechanical behaviour of the capsule wall and does not take into account the capsule reference curvature, it cannot be considered as strictly accurate. It is, however, sufficient to estimate 'how wrinkled' a capsule is. It can be noted that the absence of a reference curvature leads to a non-zero value of the curvature energy E_b^0 in the reference state.

Computing exactly the mean curvature H would require a C^2-continuous representation of the capsule wall, whereas our discretization is only *piecewise* C^2-continuous. The curvature is therefore computed approximately from the angles between the normals to contiguous elements. Each P_2 element is divided into four flat, three-node P_1 elements. Following Dyn *et al.* (2001), the mean curvature at a given node n is approximated by

$$|H_n| \approx \frac{1}{4S_n}\sum_{i=1}^{n_e} l_i|\theta_i|\,, \tag{3.10}$$

where n_e is the number of edges connected to node n, l_i is the length of edge i, θ_i is the angle between the normal vectors to the two elements connected at edge i and S_n is the Voronoi area associated with node n. The curvature energy may then take the form

$$E_b \approx \sum_{n=1}^{N_N} 2\kappa |H_n|^2 S_n. \tag{3.11}$$

4. Motion modes: tumbling and swinging

Depending on the value of the capillary number Ca, a given ellipsoidal capsule may exhibit two types of motion. At low flow strength, a 'solid-like' regime occurs, called *tumbling*. The capsule rotates like a quasi-rigid ellipsoid subjected to the flow vorticity, while the internal flow is almost stationary with respect to the membrane.

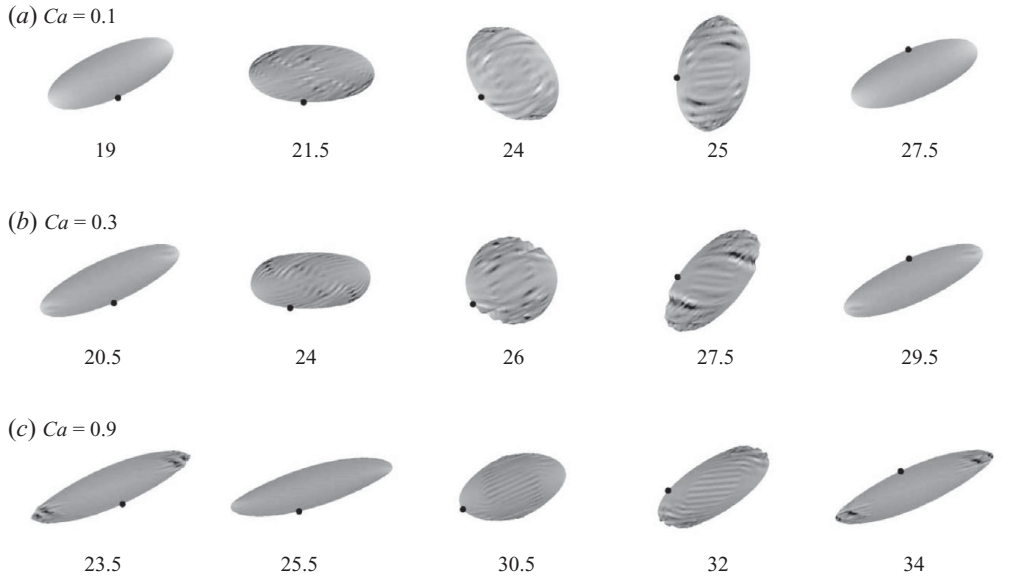

FIGURE 2. (*a*)–(*c*) Evolution of the capsule shape in the shear plane over one half-period. The initial shape is a prolate spheroid, $a/b = 2$, and the membrane follows the Sk law with $C = 1$. The grey scale corresponds to the normal component of the load, $\boldsymbol{q} \cdot \boldsymbol{n}$. The dot shows the position of material point P, originally on the short axis. The value of the non-dimensional time step $\dot{\gamma} t$ is given below each shape.

At higher flow strength, a 'fluid-like' regime occurs, called *swinging*. The membrane rotates around the deformed shape of the capsule similarly to the tank-treading motion observed for spherical capsules. Due to the initial anisotropy of the reference shape, the deformation of the capsule varies periodically with time in both regimes. As shown in figures 2 and 3, oblate and prolate spheroids both exhibit the two regimes. We now illustrate the salient features of the two types of motion for a prolate ellipsoidal capsule with initial aspect ratio $a/b = 2$ ($a/\ell = 1.59$) and an Sk membrane with $C = 1$ (figure 2). From here on, we assume the material point P to be initially on the small axis of the ellipsoid.

4.1. *Tumbling*

Figure 2(*a*) shows a tumbling capsule at different times within one half-period at $Ca = 0.1$. The capsule motion corresponds to a rigid-body rotation as illustrated by the fact that point P remains in the vicinity of its initial location. The time evolution of the characteristic angles of the motion is shown in figure 4(*a*). The angle β (measuring the major axis orientation) varies between $-\pi$ and π, which indicates that the capsule rotates like a solid body. The small oscillations of the angle δ about zero show that the material points experience small displacements about their initial position and that the membrane undergoes moderate deformation. Nevertheless, owing to the initial shape flaccidity (measured by the surface area to volume ratio), the membrane can undergo large displacements without large deformation. The large displacements are shown by the oscillation of the Taylor parameter D_{12} (figure 4*b*). The profile deformation D_{12} is maximum when the ellipsoid long axis is aligned with the straining direction of the flow, i.e. $\beta \approx \pi/4$ (figure 2*a*, $\dot{\gamma} t = 19$). This occurs for

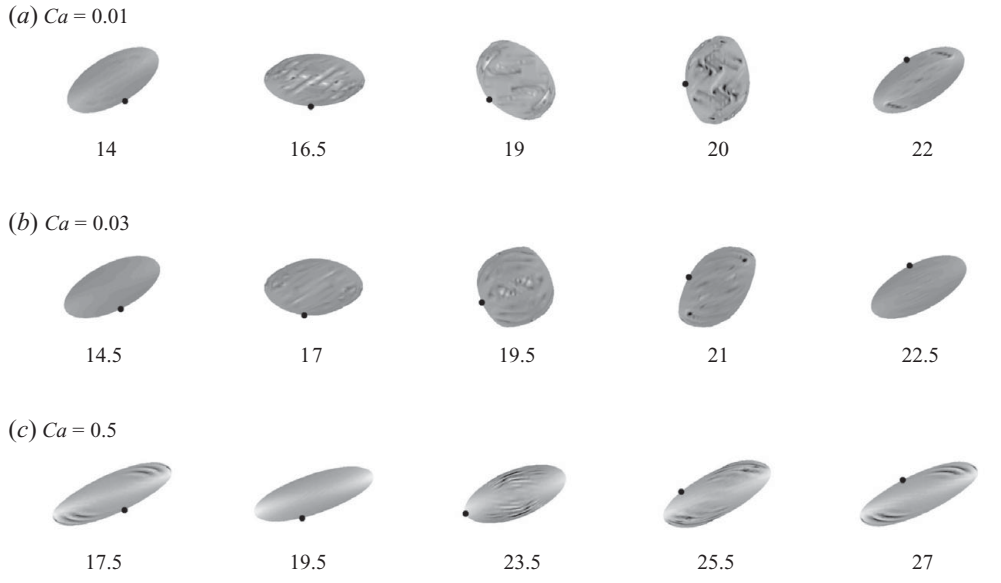

FIGURE 3. (*a*)–(*c*) Evolution of the capsule shape in the shear plane over one half-period. The initial shape is an oblate spheroid, $a/b = 0.5$, and the membrane follows the Sk law with $C = 1$. The grey scale corresponds to the normal component of the load, $\boldsymbol{q} \cdot \boldsymbol{n}$. The dot shows the position of material point P, originally on the short axis. The value of the non-dimensional time step $\dot{\gamma} t$ is given below each shape.

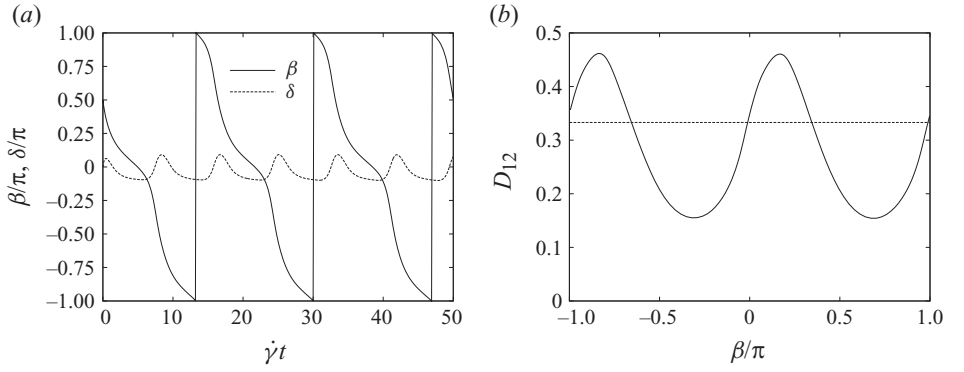

FIGURE 4. Tumbling regime (Sk law $C = 1$, $a/b = 2$, $Ca = 0.1$): (*a*) The oscillation of angle β between $-\pi$ and π indicates that the capsule rotates as a whole, whereas the small oscillation of δ shows that point P does not deviate much from its initial position. (*b*) Taylor parameter D_{12} as a function of β over one period; the initial value D_{12}^0 is indicated by the dotted line.

values of β slightly below $\pi/4$, since the flow vorticity tends to tilt the capsule in the flow direction. Such a phenomenon is also observed for initially-spherical capsules (Ramanujan & Pozrikidis 1998; Lac *et al.* 2004). Conversely, the minimum values of D_{12} are observed when the ellipsoid long axis is around $3\pi/4$ (figure 2*a*, $\dot{\gamma} t = 24$). It corresponds to the capsule position where the compression exerted by the external flow is maximum.

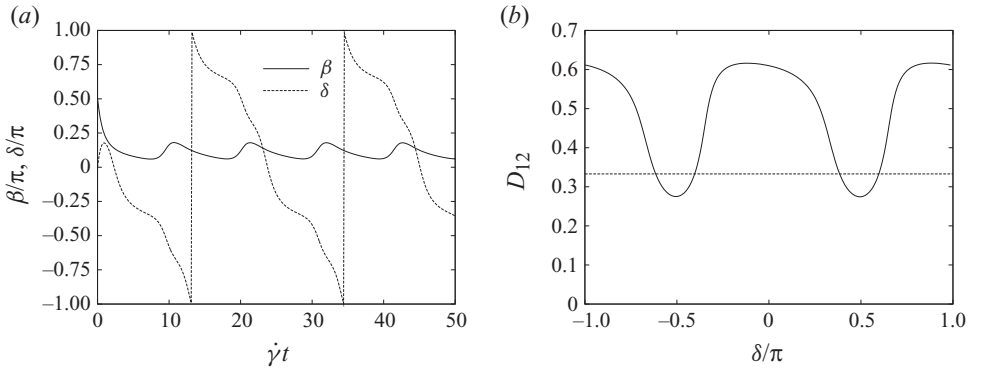

FIGURE 5. Swinging regime (Sk law $C=1$, $a/b=2$, $Ca=1.2$): (a) The small variation of β indicates that the capsule oscillates around a constant angulation, whereas the periodic variation of δ between $-\pi$ and π shows the membrane rotation. (b) D_{12} as a function of δ over one period; the initial value D_{12}^0 is indicated by the dotted line.

4.2. *Swinging*

The same capsule is now studied at a capillary number $Ca=0.9$ in the swinging regime. Figure 2(c) shows the evolution of the capsule shape at different times over one half-period. The capsule assumes an elongated shape with a long axis aligned with the maximum flow strain direction, while the membrane continuously rotates around the deformed shape. In the case of swinging, the angle β oscillates slightly around a mean value between 0 and $\pi/4$ (figure 5a). The rotation of the membrane is evidenced by the variations of the angle $\delta(t)$ between $-\pi$ and π. Figure 5(b) shows the periodic oscillation of the deformation D_{12} as a function of δ. In the swinging regime, δ can be considered as a marker of the initial position of the membrane material points (this role is played by β in the tumbling regime). The capsule reaches its maximum deformation for $\delta \approx 0, \pi$, i.e. when the material points located originally on the larger axis of the ellipsoid are in the straining direction (figure 2c, $\dot{\gamma}t=23.5$). Conversely, D_{12} is minimum when the points originally on the smaller axis are in the straining direction, or equivalently, when the points originally on the larger axis are aligned with the flow compression direction, i.e. for $\delta \approx \pm\pi/2$ ($\dot{\gamma}t=30.5$). It can be noted that D_{12} oscillates around a mean value that is larger in the swinging regime than in the tumbling regime. Such oscillations of D_{12} had previously been observed in the swinging regime for artificial capsules that were not perfectly spherical (Chang & Olbricht 1993; Walter *et al.* 2001).

4.3. *Transition*

In order to study the tumbling-to-swinging transition, we consider the same capsule ($a/b=2$) at a capillary number $Ca=0.3$. One characteristic difference between the tumbling and swinging regimes is the time evolution of the capsule long axis. In the tumbling regime, the long axis rotates over time so that $[\beta]=2\pi$; in the swinging regime, it oscillates around a mean value $\bar{\beta}$ and $[\beta]$ is small. The transition has thus been previously defined by the value of capillary number for which β no longer varies between $[-\pi, \pi]$ (Kessler *et al.* 2008; Bagchi & Kalluri 2009). However, we believe that such a criterion is not quite appropriate to determine the critical capillary number $Ca^\star$ at which the transition occurs. Indeed, figure 2(b) shows the capsule profile at various times in one half-period. During each half-cycle, the capsule takes an almost circular profile in the shear plane (here at $\dot{\gamma}t=26$). At this time, the

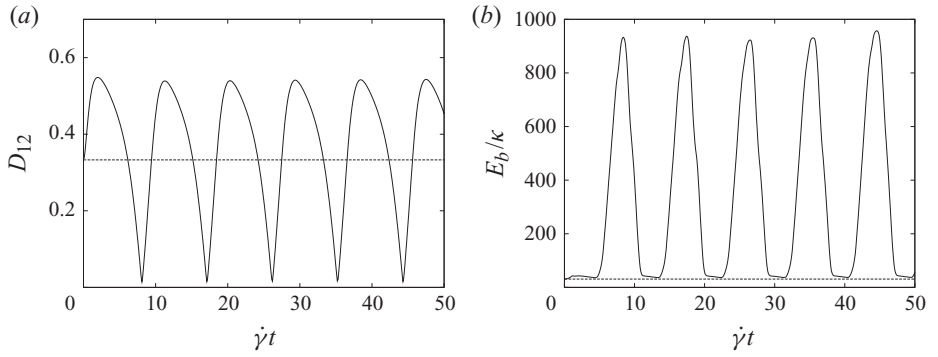

FIGURE 6. Tumbling-to-swinging transition (Sk law $C=1$, $a/b=2$, $Ca=0.3$): (a) Taylor parameter D_{12} as a function of time. (b) Approximate bending energy E_b as a function of time. In both cases, the initial value is indicated by the dotted line. The largest values of E_b correspond to the minimum values of D_{12}.

two principal axes of the ellipsoid of inertia in the shear plane have roughly the same length ($L_1 \approx L_2$), thus there is no clearly identified 'long' axis and β cannot be measured. Consequently, it is impractical to use β to determine the critical capillary number $Ca^\star$. At transition, the capsule profile becomes quasi-circular in the shear plane, so that $D_{12} \approx 0$. Thus, transition occurs when the minimum value of the Taylor parameter over one period, denoted $\min D_{12}$, becomes almost zero, as in figure 6(a). However, the shape of the capsule no longer being ellipsoidal when $D_{12} \approx 0$, the ellipsoid of inertia cannot be entirely relied upon to define the lengths of the axes. Consequently, setting the transition at the value of Ca for which $\min D_{12}$ reaches its minimum value would provide a false sense of precision. We thus propose to define the critical capillary number $Ca^\star$ as an interval using the criterion

$$\min D_{12} < 0.05. \tag{4.1}$$

This corresponds to a relative difference of 10 % between the lengths L_1 and L_2 of the axes.

Figure 2 shows that the transition is associated with an increased wrinkling of the capsule wall. The most extensive wrinkling is seen to occur as D_{12} approaches 0, i.e. as the long axis of the undeformed ellipsoid becomes shorter. To estimate the importance of wrinkles, we plot in figure 6(b) the time evolution of the approximate bending energy E_b defined in (3.9). Initially, the capsule has a small bending energy $E_b^0/\kappa = 30.9$ due only to its curved shape. A sharp increase in the bending energy occurs when D_{12} goes through its minimum value. However, wrinkling is transient during the cycle and the wrinkles disappear (E_b minimum) when the capsule long axis is in the direction of the viscous stretch ($\dot{\gamma}t = 20.5$ in figures 2b and 6b).

Having defined the transition in practical terms, let us briefly analyse it from an energetic perspective. In their semi-analytical theory, Skotheim & Secomb (2007) suppose that the shape of the capsule remains constant and postulate that the strain energy of the membrane varies as $E_m = E_m^\star \sin^2\delta$, where $E_m^\star$ is an energy barrier. The tank-treading motion occurs when the external flow transfers enough energy to the capsule membrane to reach $E_m^\star$. Otherwise, δ oscillates around 0, which corresponds to the tumbling motion. Figure 7(a) shows the actual evolution of E_m as a function of δ for two values of Ca. Slightly above transition ($Ca=0.4$), E_m is indeed maximum for $\delta = \pm\pi/2$. However, E_m does not go to 0 when $\delta \approx 0$, as postulated by the

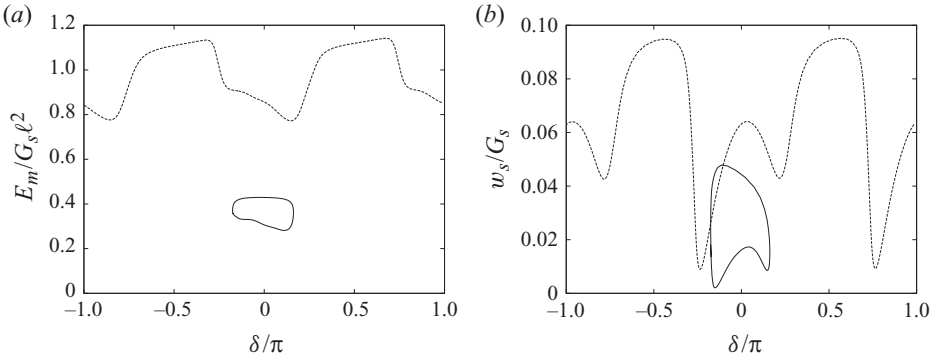

FIGURE 7. (*a*) Total strain energy of the capsule wall and (*b*) local strain energy at point P for a capsule around the tumbling-to-swinging transition. The capsule is tumbling at $Ca = 0.20$ (solid line) and swinging at $Ca = 0.40$ (dash line).

model of Skotheim & Secomb (2007). This is due to the fact that the capsule shape continuously changes over time and that the capsule is in a deformed state even when $\delta \approx 0$: its overall membrane energy is therefore never zero. Since the transition occurs when material points initially on the short axis of the capsule manage to go on to the long axis, it is interesting to consider the energy per unit area w_s of the material point P, as shown in figure 7(*b*). In the swinging case ($Ca = 0.4$), the energy of point P is maximum when $\delta = \pm \pi/2$, i.e. when the material point, initially on the short axis, moves on to the long axis. For the transition to occur, the critical stage for point P is to have enough energy to go beyond $\delta = \pm \pi/2$. This is not the case at $Ca = 0.2$: point P moves away from its initial position, but returns towards it when the energy associated with the membrane deformation equals the total available energy. It thus appears that the transition can be understood as the crossing of an energy barrier as proposed by Skotheim & Secomb (2007). However, the energy variation with respect to δ is more complex than predicted in the theoretical model because the capsule shape changes over time.

4.4. *Effect of capsule shape*

In the following sections, all studies are conducted for two initial values of the aspect ratio: $a/b = 0.5$ (oblate spheroid) and $a/b = 2$ (prolate spheroid). These two aspect ratios are well-suited for comparing the influence of the capsule initial shape. The two spheroids have, by definition, the same internal volume and therefore the same length scale, l. With initial surface areas differing by less than 2 %, the two capsules essentially have the same initial value of the surface-area-to-volume ratio. They also share the same initial value for the Taylor parameter in the shear plane ($D_{12}^0 = 0.33$). Any difference in their behaviour is then only due to the difference in their initial geometry in the orthogonal direction. As shown in figures 2 and 3, the behaviours of the two types of capsules are qualitatively similar; tumbling and swinging occur in both cases. Quantitative differences exist, however, which are detailed in the following sections.

5. Influence of the capillary number and material law

We now conduct a systematic study of the motion of a spheroidal capsule in a simple shear flow as a function of the capillary number. Two material laws are used to describe the membrane, the neo-Hookean law (2.10) and Skalak's law (2.11) with

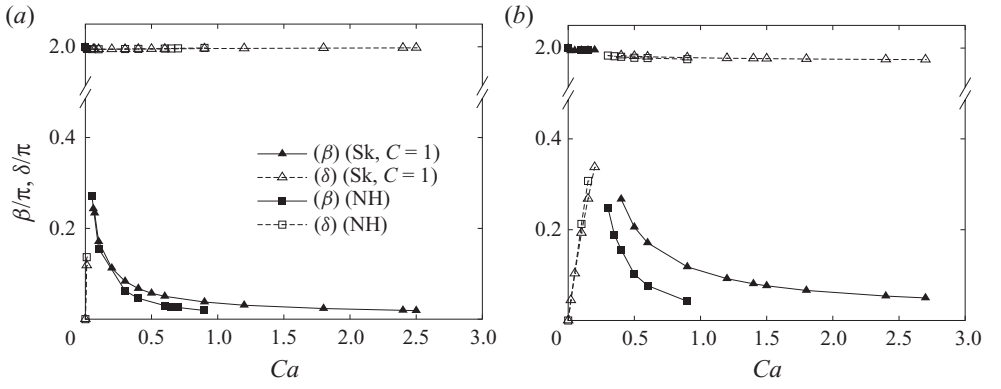

FIGURE 8. Peak-to-peak amplitude of the oscillations of the angles β and δ for two initial shapes and two material laws. (*a*) Oblate spheroid, $a/b = 0.5$. (*b*) Prolate spheroid, $a/b = 2.0$.

$C = 1$, which have the same behaviour at small deformations. Two initial aspect ratios are studied: $a/b = 0.5$ and $a/b = 2$. This makes it possible to compare the behaviour of oblate and prolate spheroids, but a systematic study of the influence of the aspect ratio is outside the scope of this article.

5.1. *Kinematics*

Figure 8 shows the peak-to-peak amplitudes of the angles β and δ for the two initial shapes and material laws. The general evolution of the angles depends only moderately on the capsule initial shape (oblate/prolate), but strongly on the motion regime (tumbling/swinging). No data are shown in the interval of the transition, since the angles can no longer be determined accurately as discussed in § 4.3. During the tumbling regime ($[\beta] = 2\pi$), the oscillations $[\delta]$ increase with Ca. This means that the membrane deformation oscillation increases with flow strength. In the swinging regime, as the membrane tank-treads around the capsule ($[\delta] = 2\pi$), the amplitude $[\beta]$ of the oscillation of the capsule inclination decreases with Ca. Indeed, as the capsule gets more deformed, the influence of the initial ellipsoidal shape fades out and the capsule behaviour tends towards that of an initially-spherical capsule (constant angle β).

We show the minimum value $\min D_{12}$ as a function of Ca and membrane law in figure 9. It is clear that $\min D_{12}$ indeed goes through a global minimum in all cases. The criterion $\min D_{12} < 0.05$ provides values of $Ca^\star$ confined within a small interval, because of the sharp variations of $\min D_{12}$ around the global minimum. To determine the intervals for the critical capillary number $Ca^\star$, the capillary number was increased systematically by steps of 0.01 for oblate spheroids and by steps of 0.05 for prolate spheroids. The values of capillary number for which $\min D_{12} < 0.05$ are provided in table 1. Note that, for a given aspect ratio, the $Ca^\star$ intervals are almost equal for the two material laws considered. This is due to the fact that the transition takes place at moderate deformation levels, for which the two laws behave similarly. However, oblate and prolate capsules have values of $Ca^\star$ that differ by a factor ~ 10 in order of magnitude. This point will be discussed in § 7.2.

In order to evaluate the influence of the capsule material law and initial shape on deformation, we plot $\bar{D}_{12}$ and the mean axis length $\bar{L}_3/\ell$ along $\mathbf{e}_3$ as functions of Ca for the two laws and the two initial shapes in figure 10. Only in the tumbling regime, can a difference be observed between oblate and prolate capsules. Indeed, oblate capsules experience an initial decrease in $\bar{D}_{12}$ with Ca, whereas in the swinging

	$a/b = 0.5$	$a/b = 1$	$a/b = 2$
NH	$Ca^\star \in [0.02, 0.04]$ $Ca_H = 0.70$	$\star$ $Ca_H = 0.63$	$Ca^\star \in [0.20, 0.25]$ $Ca_H = 0.35$
Sk, $C = 1$	$Ca^\star \in [0.02, 0.05]$ $Ca_H = 2.5$	$\star$ $Ca_H = 2.4$	$Ca^\star \in [0.25, 0.35]$ $Ca_H = 1.4$

TABLE 1. Values of the critical capillary numbers $Ca^\star$ and Ca_H for the cases studied. The values of Ca_H are provided for an initially-spherical capsule for reference (as given by Lac *et al.* 2004).

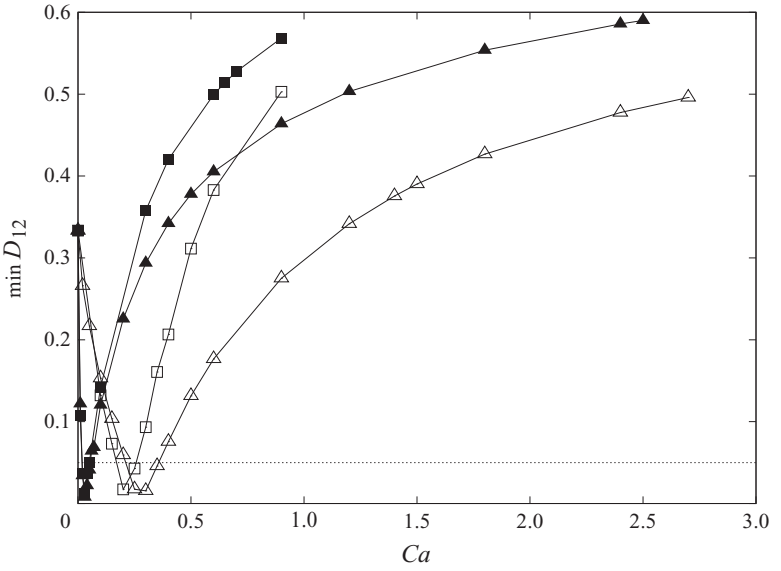

FIGURE 9. Minimum value of the Taylor parameter over one period for an oblate spheroid ($a/b = 0.5$, filled symbols) and a prolate spheroid ($a/b = 2$, open symbols). □: NH law; △: Sk law with $C = 1$. The horizontal line corresponds to the limit $\min D_{12} = 0.05$ used to define the transition.

regime, $\bar{D}_{12}$ increases with Ca in both cases, while the influence of initial shape eventually fades out. A larger value of Ca is required to reach the same value of $\bar{D}_{12}$ with the Sk law than with the NH law. If the NH and Sk ($C = 1$) laws behave similarly at small deformation levels, they are known to diverge at larger deformation, the Sk law exhibiting a strain-hardening behaviour and the NH law a strain-softening one. As shown in figure 10(b), $\bar{L}_3/\ell$ tends towards a constant value when Ca increases for the Sk law. The deformation induced by the shear flow therefore occurs mainly along the profile in the shear plane (x_1, x_2). No such convergence is found for the NH law.

5.2. *Membrane tensions*

It is shown in figure 2 that widespread in-plane compression can occur. In the absence of a physical bending stiffness in the numerical model, such compressive tensions cause numerical wrinkles. In order to study in-plane compression, figures 11 and 12 show the minimum principal tension denoted $\tau_{min}(t)$ and its maximum value

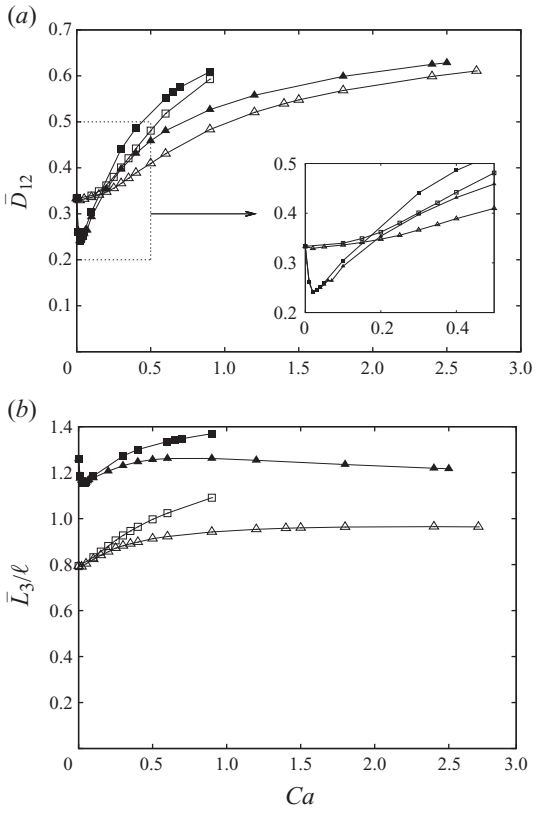

FIGURE 10. Mean values of the Taylor parameter $\bar{D}_{12}$ (*a*) and semi-diameter $\bar{L}_3$ (*b*) of the ellipsoid of inertia for an oblate spheroid ($a/b = 0.5$, filled symbols) and a prolate spheroid ($a/b = 2$, open symbols). □: NH law; △: Sk law with $C = 1$.

over one period denoted $\max \tau_{min}$,

$$\max \tau_{min} = \max_t(\tau_{min}(t)) = \max_t \left(\min_{\boldsymbol{x}, i=1,2} (\tau_i(\boldsymbol{x}, t)) \right), \tag{5.1}$$

where τ_i are the principal tensions. In all the cases studied, τ_{min} is negative through most of the period indicating that compression always occurs somewhere for spheroidal capsules (see examples in figure 11). The positive values of τ_{min} occur when the long axis of the original ellipsoid is in the straining direction, i.e. $\beta \approx \pi/4, -3\pi/4$ in the tumbling regime and $\delta \approx 0, -\pi$ in the swinging regime.

Figure 12 shows that, for large values of Ca, even the maximum value of τ_{min} is negative. It means that negative tensions occur even when the capsule reaches its maximum elongation. The reason is that, at large values of Ca, negative tensions and wrinkles appear at the tips of the elongated capsule (figure 13). Lac *et al.* (2004) observed this phenomenon for an initially-spherical capsule and defined Ca_H as the capillary number above which negative tensions appear at steady state. In the case of spheroidal capsules, we define Ca_H as the critical capillary number above which $\max \tau_{min} < 0$. The values of Ca_H found for the different cases studied are provided in table 1.

In order to estimate the amount of wrinkling caused by the negative tensions, the maximum value of the approximate curvature energy E_b over one period is shown

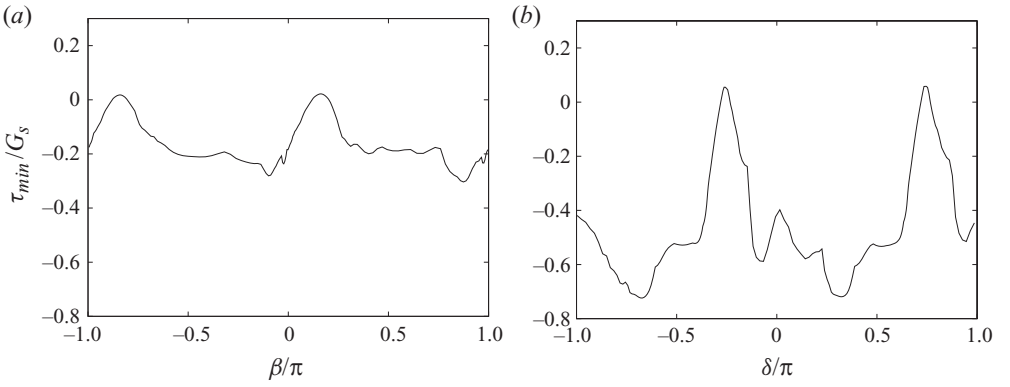

FIGURE 11. Minimum principal tension as a function of the angles β and δ. The capsule is a prolate spheroid ($a/b = 2$) and the membrane follows the Sk law with $C = 1$. (a) Tumbling regime, $Ca = 0.1$; (b) swinging regime, $Ca = 0.9$.

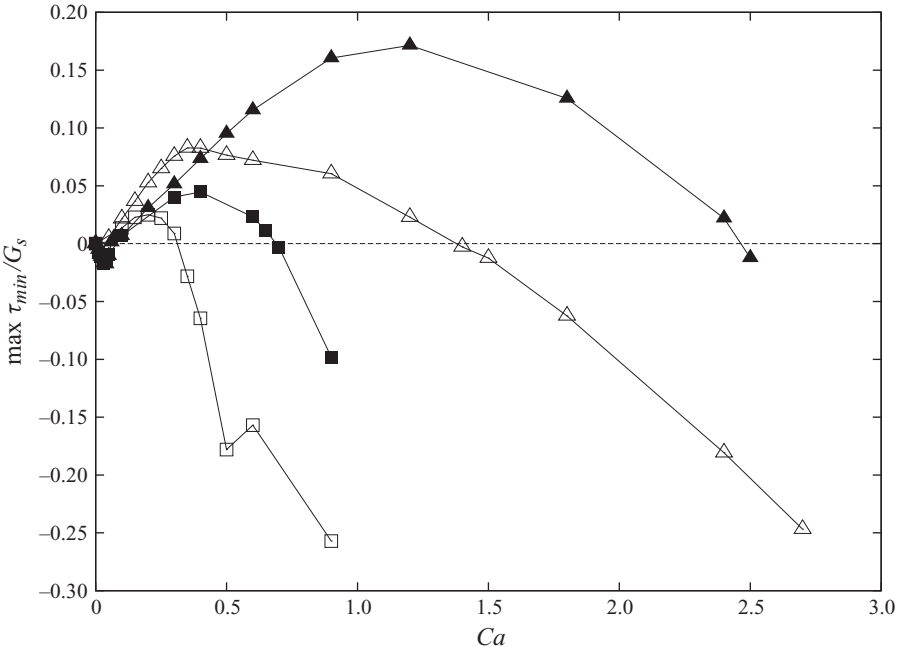

FIGURE 12. Maximum value during a period of the minimum principal tension for an oblate spheroid ($a/b = 0.5$, filled symbols) and a prolate spheroid ($a/b = 2$, open symbols). □: NH law; △: Sk law with $C = 1$.

in figure 14. For all values of Ca, max E_b is far above the value computed for the initial shape ($E_b^0/\kappa = 33.8$ and 30.9 for oblate and prolate spheroids, respectively). This confirms that the capsule undergoes large wrinkling during motion. Except for a prolate NH spheroid, the largest amount of wrinkling occurs in the swinging regime, for values of Ca slightly above $Ca^\star$. During tank-treading motion, strong wrinkling tends to occur when $\delta \approx \pi/2$, i.e. when the long axis of the initial ellipsoid has to be compressed to become the short axis of the deformed capsule. However, as the capillary number is increased and the capsule becomes more elongated, the

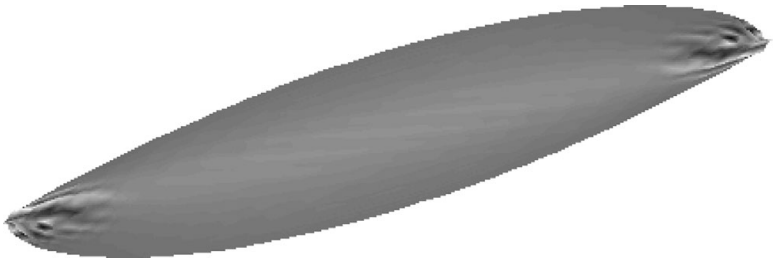

FIGURE 13. Elongated capsule ($a/b = 2$) buckling at the tips when $Ca = 1.8 > Ca_H$ and the elongation is maximum ($\delta \approx 0$). The membrane follows the Sk law with $C = 1$.

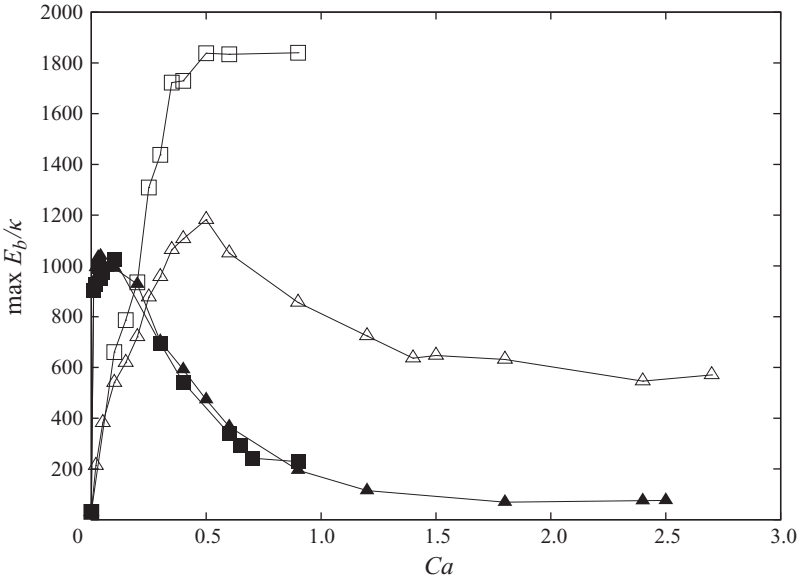

FIGURE 14. Maximum value during a period of the approximate curvature energy for an oblate spheroid ($a/b = 0.5$, filled symbols; $E_b^0/\kappa = 33.8$) and a prolate spheroid ($a/b = 2$, open symbols; $E_b^0/\kappa = 30.9$). □: NH law; △: Sk law with $C = 1$.

isotropic component of the tensions (related to the Poisson ratio of the membrane) increases and compensates the negative tensions at $\delta \approx \pi/2$; wrinkling then becomes less important. The maximum amount of wrinkling therefore occurs during transition and for capillary numbers slightly above it.

In the case of a prolate NH spheroid, the wrinkling does not subside as Ca increases. This is a consequence of the proximity of the two critical capillary numbers $Ca^\star \in [0.20, 0.25]$ and $Ca_H = 0.35$ in this particular case. Indeed, if we consider a material point originally on the long axis of the ellipsoid, at $Ca \approx 0.35$, when $\delta \approx \pi/2$, the point is on the short axis of the deformed capsule and strong wrinkling occurs, since Ca is only slightly above $Ca^\star$. A quarter of a period later, the material point is in the straining direction, but buckling and wrinkling occur at the tips, as Ca is around Ca_H. These two phenomena then lead to a constant wrinkling of the membrane, that even seems to amplify over time, but this is probably a numerical artefact due to the lack of a proper bending stiffness in the model of the capsule wall.

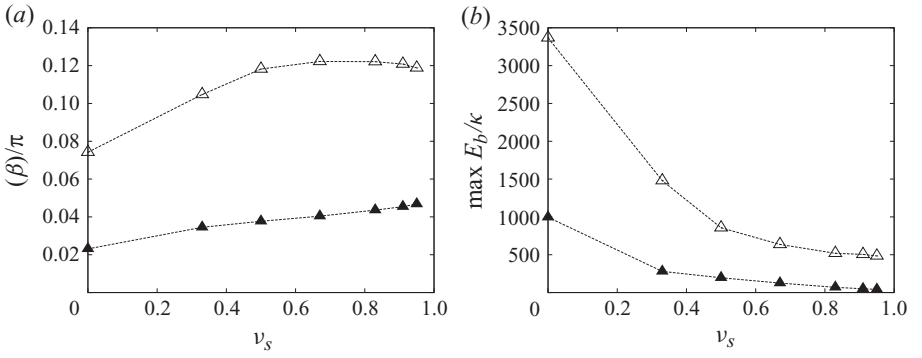

FIGURE 15. Amplitude of the oscillations of (a) the inclination angle β, (b) the Taylor parameter and (c) the maximum of the approximate curvature energy as a function of the Poisson ratio at $Ca = 0.9$ for an oblate spheroid ($a/b = 0.5$, filled symbols) and a prolate spheroid ($a/b = 2$, open symbols). The membrane follows the Sk law.

6. Influence of the areaa dilatation modulus

In § 5, we have studied two material laws that have the same behaviour at small deformations, corresponding to $K_s = 3G_s$, or equivalently to a Poisson ratio $\nu_s = 0.5$. To study the influence of the area dilatation modulus, we now vary the ratio K_s/G_s by using Skalak's law and changing the value of the parameter C. The two quantities are related by $K_s/G_s = 1 + 2C$, so that $\nu_s = C/(1 + C)$. In the following study, C is varied within the range $0 \leqslant C \leqslant 20$, which corresponds to $1 \leqslant K_s/G_s \leqslant 41$ and $0 \leqslant \nu_s \leqslant 0.95$. Negative or zero values of $\nu_s = 0$ correspond to materials that are naturally wrinkled perpendicularly to the membrane plane and that expand (or keep the same length if $\nu_s = 0$) in the direction orthogonal to the uniaxial extension one. Values of ν_s near unity correspond to a membrane that is almost area-inextensible.

6.1. *Influence of ν_s on the swinging regime*

We first study the influence of C at a given value of the capillary number, $Ca = 0.9$, for the two aspect ratios $a/b = 0.5$ and $a/b = 2$. For all the values of C considered, the capsule is in the swinging regime.

As ν_s is increased, the capsule becomes stiffer and deforms less. Consequently, the mean value of the Taylor parameter $\bar{D}_{12}$ decreases, the mean value of the inclination angle $\bar{\beta}$ increases and the tank-treading period T decreases. These results are well known for initially-spherical capsules (Lac *et al.* 2004; Li & Sarkar 2008) and are therefore not shown here.

We concentrate instead on the amplitudes of the oscillations of these quantities. As shown in figure 15(a), the oscillations of the inclination angle do not disappear when ν_s increases, and even tend to increase for oblate spheroids. This is consistent with the observations of Abkarian *et al.* (2007) on red blood cells ($\nu_s \approx 1$), which have been seen to oscillate in a simple shear flow. We also estimate the effect of the Poisson ratio on the amount of wrinkling in figure 15(b). It indicates that the maximum of the approximate bending energy $\max E_b$ decreases sharply as ν_s increases. Higher values of ν_s increase the importance of the isotropic part of the tensions, leading to decreased wrinkling when $\delta \approx \pm \pi/2$. This is consistent with the reasoning given in § 5.2.

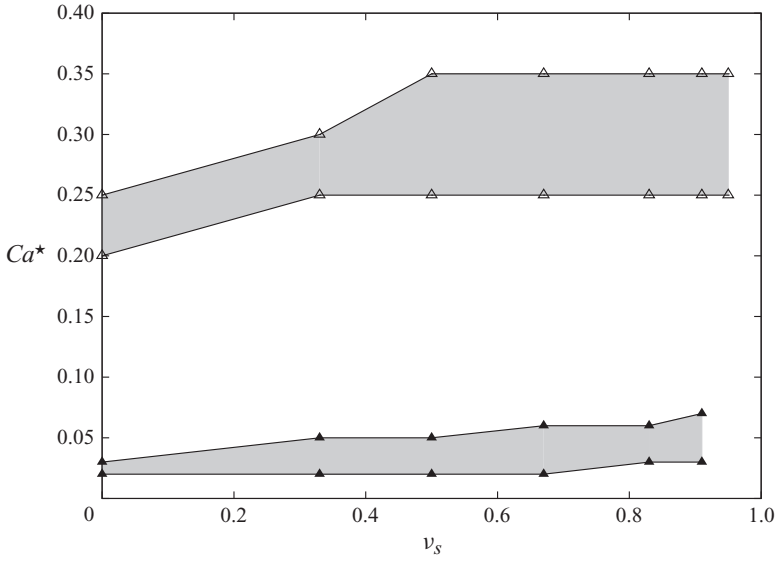

FIGURE 16. Range of values of the transition capillary number $Ca^\star$ as a function of the Poisson ratio for an oblate spheroid ($a/b = 0.5$, filled symbols) and a prolate spheroid ($a/b = 2$, open symbols). The membrane follows the Sk law.

6.2. *Influence of ν_s on the tumbling-to-swinging transition*

We now look at the range of values of the capillary number for which the tumbling-to-swinging transition occurs, as defined by (4.1). The ranges, shown in figure 16, are determined by increasing Ca by steps of 0.01 when $a/b = 0.5$ and steps of 0.05 when $a/b = 2$. It is remarkable that the intervals for $Ca^\star$ depend only moderately on the area dilatation modulus. For instance, for $a/b = 2$, when C is increased from 0 to 20, the ratio K_s/G_s is multiplied by 41, but $Ca^\star$ only increases by approximately 30 %. $Ca^\star$ is even found to remain constant for $\nu_s \geqslant 0.5$. Similar results are found for $a/b = 0.5$. It shows that most capsules have a tumbling-to-swinging transition that hardly depends on the area dilatation modulus K_s regardless of the material they are made of. The main capsule mechanical property that governs the transition is thus its shear modulus G_s.

In order to understand this phenomenon, one can consider the energy barrier described in § 4.3 that the capsule has to cross to go from tumbling to swinging. Figure 17 shows the membrane strain energy E_m for a value of Ca slightly above $Ca^\star$ when $\nu_s = 0.5$ along with its decomposition into a shear term E_m^G and an area dilatation term E_m^K, as defined by (3.8). It is apparent that the energy barrier at $\delta = \pm \pi/2$ consists mainly of shear energy E_m^G, which explains why the transition depends much more on the value of G_s than on K_s. It can therefore be surmised that the intervals for $Ca^\star$ would not differ much from the values obtained here if an area-incompressible capsule wall were considered.

7. Discussion

We have modelled the behaviour and large deformation of an ellipsoidal capsule in a simple shear flow using the novel method of Walter *et al.* (2010), that couples boundary integrals for the flows to finite membrane elements. The study has shown that the coupling method is well-suited to the simulation of non-spherical capsules and that it

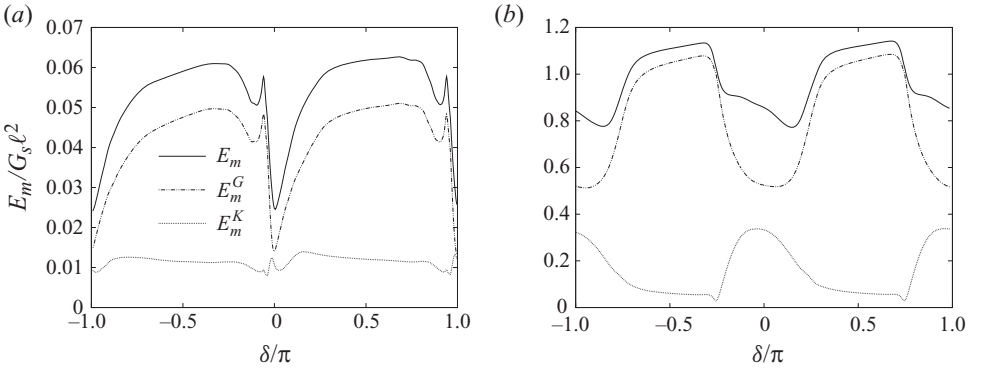

FIGURE 17. Strain energy function E_m of the capsule wall slightly above the transition and its decomposition into a shear term E_m^G and an area dilatation term E_m^K. The energy barrier at $\delta = \pm \pi/2$ consists mainly of shear energy. (*a*) Oblate spheroid, $a/b = 0.5$, $Ca = 0.06$; (*b*) prolate spheroid, $a/b = 2.0$, $Ca = 0.4$. The membrane follows the Sk law with $C = 1$.

remains numerically stable even in the presence of in-plane compression. It allowed us to study the behaviour of oblate and prolate spheroids, with aspect ratios $a/b = 0.5$ and $a/b = 2$, and to recognize two regimes: a quasi-solid regime ('tumbling') and a quasi-fluid regime ('swinging'). Oblate and prolate spheroids behave qualitatively similarly in most respects, apart from the tumbling-to-swinging transition, which occurs at a much lower value of Ca for oblate spheroids. We also studied the effect of a variation of the Poisson ratio on the behaviour of the capsule. While it has a quantitative impact on several characteristics of the motion, it only marginally changes the capillary number $Ca^\star$ at which the transition occurs. We now discuss three important questions raised by our study: the definition and number of mechanical regimes that exist for the cases studied, the similarities and differences between oblate and prolate spheroids and the importance of the bending stiffness of the capsule wall.

7.1. *Regimes*

In this study, two distinct regimes are found: the *tumbling* regime at low capillary numbers where the long axis of the capsule rotates in the shear plane and the *swinging* regime at high capillary numbers where this axis oscillates around a mean inclination and membrane rotation (tank treading) occurs. These two regimes are separated by a transition region, during which the capsule transits through a phase where the two axes of the capsule in the shear plane are approximately of the same length ($D_{12} \approx 0$). We do not believe that the transition can be considered as a separate regime, distinct from tumbling and swinging. It rather corresponds to the parameter range where the two regimes behave so closely that they cannot be accurately distinguished from one another.

In their systematic study of the behaviour of ellipsoidal capsules, Kessler *et al.* (2008) also found a transition during which $D_{12} \approx 0$. However, they defined the inclination angle of the long axis for all the capillary numbers. The angle was then used to determine the exact value of the capillary number at transition. Bagchi & Kalluri (2009) did likewise and, in the cases where $D_{12} \approx 0$, they found that the inclination angle could become negative; they defined this behaviour as a separate regime, which they termed vacillating–breathing. In the present study, we have chosen to refrain from using the axes and angles computed by using the ellipsoid of inertia when the Taylor parameter is lower than 0.05. This arbitrarily-chosen value corresponds to a

relative difference of 10 % between the lengths of the principal axes of the ellipsoid of inertia in the shear plane. We strongly believe that, when the lengths of the axes become very similar, a long axis can no longer be defined and the inclination angle computed with the ellipsoid of inertia is no longer meaningful. We are therefore unable to give exact values of Ca at transition or to comment on the existence of the vacillating—breathing regime, as those fall into the range for which the capsule shape can no longer be analysed accurately.

Along with the present study, all the existing numerical studies of capsules in simple shear flow indicate that the tumbling-to-swinging transition is associated with a phase when $D_{12} \approx 0$ (Kessler *et al.* 2008; Sui *et al.* 2008; Bagchi & Kalluri 2009). The semi-analytical study of Finken *et al.* (2010) also leads to a transition with $D_{12} \approx 0$. A similar behaviour has been found experimentally for lipid vesicles (Kantsler & Steinberg 2006; Deschamps, Kantsler & Steinberg 2009). These findings are, however, at odds with the experiments conducted by Abkarian *et al.* (2007) on red blood cells in a simple shear flow. They observe that, during the tumbling-to-swinging transition, the red blood cell maintains an almost constant shape and that the transition occurs through an *intermittent regime* during which the cell alternately swings and tumbles. The analytical theory of Skotheim & Secomb (2007), which assumes that the capsule shape remains constant, also finds this intermittent regime. However, our study and the other numerical studies cited above fail to find such an intermittent regime and always observe that the tumbling-to-swinging transition is associated with large variations of the capsule shape. One possible explanation is that the time during which a red blood cell assumes the shape with $D_{12} \approx 0$ is so short that it may be missed experimentally. Another possibility is that a key component of the mechanical properties of a red blood cell is missing in the numerical models, leading to major differences in the behaviour. Maintaining a quasi-constant shape, through a mechanism yet to be determined, may be the key to the existence of the intermittent transition regime. One should bear in mind that the red blood cell is a very complex kind of capsule; experimental data on artificial capsules with simple protein membranes and non-spherical reference shapes are sorely needed to further investigate this question.

7.2. *Influence of capsule initial geometry*

Two initial aspect ratios were considered and it has been shown in § 5 that the behaviours of these two types of capsules are qualitatively similar; tumbling and swinging are observed for both types of capsules, separated by a transition zone. Only moderate quantitative differences are found, which can be explained by the great similarity in the geometric properties of the initial shapes. The theoretical model by Keller & Skalak (1982) sheds some light on the detailed reasons behind such similarities. They extended the analysis conducted by Jeffery (1922) on rigid ellipsoids and showed that, for a capsule maintaining a constant ellipsoidal shape during deformation, the energy dissipation in the fluids is a function of three non-dimensional geometric parameters given in the case of spheroids by

$$f_1 = 4z_1^2, \quad f_2 = 4z_1^2\left(1 - \frac{2}{z_2}\right), \quad f_3 = -4\frac{z_1}{z_2}, \tag{7.1}$$

where

$$z_1 = \frac{1}{2}\left|\frac{a}{b} - \frac{b}{a}\right|, \quad z_2 = \left(\tilde{a}^2 + \tilde{b}^2\right) g_3', \tag{7.2}$$

	a/ℓ	b/ℓ	A/ℓ^2	f_1	f_2	f_3	$1/f_3$	$\frac{f_3}{f_2-f_1}$
$a/b=0.5$	0.63	1.26	13.8	2.25	−2.39	−3.09	−0.32	0.67
$a/b=2$	1.59	0.79	13.5	2.25	−3.38	−3.76	−0.27	0.67

TABLE 2. Initial values of the geometric characteristics of the capsules for two aspect ratios: lengths of the axes a, b, surface area A, non-dimensional parameters f_i used to compute the energy dissipation in the fluids.

770 with

$$g_3' = \int_0^\infty \frac{\mathrm{d}s}{(\tilde{a}^2+s)^{\frac{3}{2}}(\tilde{b}^2+s)^2}\,, \quad \tilde{a}=a/\ell\,,\tilde{b}=b/\ell. \tag{7.3}$$

771 As shown in table 2, the values of these geometric parameters are close or identical
772 for the two shapes considered. The external flow can therefore be expected to act
773 in a similar way on the two capsules at a given capillary number. The analytical
774 model by Keller & Skalak (1982) has then been extended by Skotheim & Secomb
775 (2007) to include the effect of the membrane elasticity. Assuming similarly that the
776 capsule maintains a constant shape, the latter found that the equations of motion are
777 affected (for $\lambda=1$) by the geometry of the capsule through four terms, $ab/(a^2+b^2)$,
778 $|a^2-b^2|/(a^2+b^2)$, $1/f_3$, $f_3/(f_2-f_1)$ and by the elastic energy $E_m^\star$. They defined the
779 elastic energy $E_m^\star$ as the energy barrier at the tumbling-to-swinging transition. When
780 using the initial values of a/ℓ and b/ℓ, we find that the first two terms are strictly
781 equal for the two aspect ratios considered here and the following two have similar
782 values, as shown in table 2. The analytical theory by Skotheim & Secomb (2007) is
783 therefore consistent with the fact that the two capsules generally behave similarly.
784 However, an important difference is found. The tumbling-to-swinging transition
785 occurs at much lower values of the capillary number for the oblate spheroid
786 ($Ca^\star \in [0.02, 0.05]$ for the Sk law with $C=1$) than for the prolate spheroid
787 ($Ca^\star \in [0.25, 0.35]$). To understand this discrepancy, one must consider the fifth
788 parameter, i.e. the elastic energy $E_m^\star$. For the Sk law with $C=1$, we define $E_m^\star$
789 as the maximum value of E_m over one period and evaluate it at $Ca=0.03$ for
790 $a/b=0.5$ and at $Ca=0.3$ for $a/b=2.0$. We find

$$E_m^\star/(G_s\ell^2) = 0.025, \quad a/b=0.5, \tag{7.4}$$

791 and

$$E_m^\star/(G_s\ell^2) = 0.75, \quad a/b=2. \tag{7.5}$$

792 The values differ substantially for the two aspect ratios considered, a much lower
793 energy being necessary to reach the shape for which $D_{12}\approx 0$ for the initially-oblate
794 spheroid than for the initially-prolate one.
795 In conclusion, we have shown that, for a given capillary number, the energy
796 brought by, and dissipated in, the flows is of the same order for both aspect ratios,
797 and therefore so is the energy E_m stored in the capsule membrane. However, the value
798 that E_m has to reach for the tumbling-to-swinging transition to take place depends
799 strongly on whether the capsule is oblate or prolate. This is why the transition occurs
800 at much lower values of Ca for the oblate than for the prolate capsule.
801 It may be noted that the bending stiffness of the capsule wall has been neglected
802 both in the numerical simulations and in the theory presented in this section, and
803 one may wonder how it could affect its conclusions. It has indeed been noted in § 4.3

that the capsule shapes at transition are strongly wrinkled for both aspect ratios. To investigate this point, we have quantified the approximate curvature energy $E_b^\star$ at transition and found

$$E_b^0/\kappa = 33.8\,, \quad E_b^\star/\kappa = 970, \quad a/b = 0.5, \tag{7.6}$$

and

$$E_b^0/\kappa = 30.9\,, \quad E_b^\star/\kappa = 950 \quad a/b = 2. \tag{7.7}$$

As the approximate curvature energy $E_b^\star$ at transition is similar in the two cases, we can conclude that the amount of wrinkling does not depend on the capsule initial geometry. Therefore, it can be surmised that taking into account the bending stiffness in the mechanical model of the capsule wall would not have changed the fact that the transition occurs at much lower capillary numbers for oblate than for prolate spheroids.

7.3. *Influence of bending stiffness*

In this work, we have used a novel numerical technique coupling a finite element and a boundary integral method (Walter *et al.* 2010). The method is found to remain stable despite the large compressive tensions that appear in the membrane of the ellipsoidal capsules during their deformation. The presence of compressive tensions is a particularl3nsitive issue for non-spherical capsules. For spherical capsules in a simple shear flow, there exists a range of capillary numbers in which a steady state free of compression can be attained. It is not so for ellipsoidal capsules: compression is always present for at least part of a period (i.e. $\min \tau_{min} < 0$) and zones where compression occurs tend to be more widespread. We believe that the numerical stability in the presence of in-plane compression is achieved thanks to the stiffness brought by the finite elements. This stiffness is purely numerical; for instance, when wrinkles appear, their wavelength is determined by the sq of the mesh. Since it does not obey a mechanical law, this stiffness cannot be expected to model the buckling of a real capsule accurately.

The membrane model presently used is therefore not sufficient to predict the exact *local* behaviour of the capsule wall when compression occurs. It is, however, sufficient to determine the zones where compression occurs. As shown in figure 18, a reduction in the mesh size changes accordingly the wavelength of the wrinkles but affects neither the general shape of the capsule nor the location of the compressive tensions. It therefore appears that the model used in this work is a reasonably good approximation of a real capsule with a very small bending stiffness. In this case, results such as the location of negative tensions or the Taylor parameter computed with this model can be trusted. For capsules with a large bending stiffness, a numerical model incorporating resistance to bending is necessary.

Of particular interest is the case of the tumbling-to-swinging transition, as wrinkling is especially strong during this phase. It is important to determine whether the bending stiffness can change the value of the capillary number for which transition occurs. For the bending effects to have a negligible influence on the transition, the curvature energy of the transition shape $S^\star$ must be negligible compared to the membrane energy, i.e.

$$E_b^\star \ll E_m^\star. \tag{7.8}$$

Using the non-dimensional values of $E_m^\star/G_s\ell^2$ and $E_b^\star/\kappa$ given in § 7.2 for $a/b = 0.5$, (7.8) leads to $\kappa/G_s\ell^2 \ll 2.6 \times 10^{-5}$. To provide an experimental interpretation of this condition, let us consider an artificial capsule with a wall made of a thin sheet

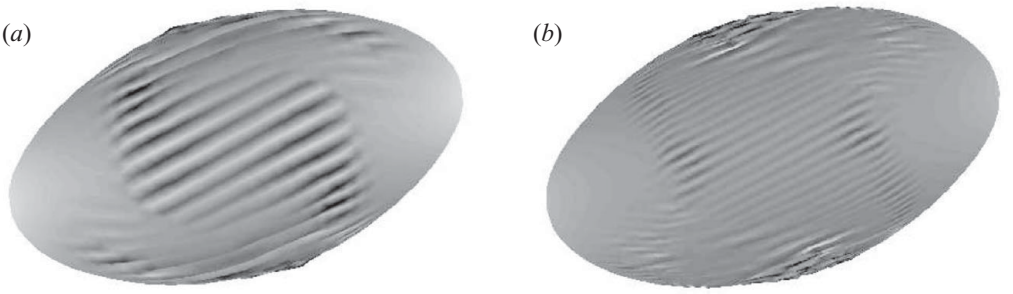

FIGURE 18. Prolate ellipsoid at $Ca = 0.9$ meshed with (a) 1280 and (b) 5120 P_2 elements. When the mesh size is divided by 2, so is the wavelength of the wrinkles, but the overall shape of the capsule is not affected.

of fully-isotropic elastic material. The bending modulus is then $\kappa = G_s\vartheta^2/6(1-\nu_s)$, where ϑ is the initial thickness of the capsule wall, and the condition on the bending modulus can be replaced by that on the thickness

$$\vartheta/\ell \ll 9 \times 10^{-3}. \tag{7.9}$$

This value may be compared with the data available for spherical artificial capsules. For instance, Risso, Collé-Paillot & Zagzoule (2006) report $\vartheta/\ell = 2 \times 10^{-2}$ for the alginate/human–serum–albumin capsules that they used, while the ovalbumin microcapsules used by Lefebvre *et al.* (2008) have $\vartheta/\ell = 3 \times 10^{-3}$.

Therefore, neglecting the bending stiffness of the capsule wall, as done in this work, can provide reliable results for certain types of capsules, especially far from the transition when wrinkling is less important.

A theoretical study of the wrinkling of a spherical capsule in a shear flow was performed by Finken & Seifert (2006) for cases where regular wrinkles with a small wavelength develop on the membrane. This analytical study does not cover all the complex buckling patterns observed in figures 2 and 3 for non-spherical capsules. To the best of our knowledge, a full numerical study exploring the effect of the bending modulus on the motion and large deformation of a capsule (spherical or not) in flow remains to be conducted. In particular, if one is interested in drawing up a phase diagram showing the different types of motion of an ellipsoidal capsule, the bending stiffness of the wall will need to be included as a parameter of the diagram.

REFERENCES

ABKARIAN, M., FAIVRE, M. & VIALLAT, A. 2007 Swinging of red blood cells under shear flow. *Phys. Rev. Lett.* **98** (18), 188302.

BAGCHI, P. & KALLURI, R. M. 2009 Dynamics of nonspherical capsules in shear flow. *Phys. Rev.* E **80** (1), 016307.

BARTHÈS-BIESEL, D. 2003 Flow-induced capsule deformation. In *Modelling and Simulation of Capsules and Biological Cells*, pp. 1–31. Chapman & Hall/CRC.

BARTHÈS-BIESEL, D., DIAZ, A. & DHENIN, E. 2002 Effect of constitutive laws for two dimensional membranes on flow-induced capsule deformation. *J. Fluid Mech.* **460**, 211–222.

BARTHÈS-BIESEL, D. & RALLISON, J. M. 1981 The time-dependent deformation of a capsule freely suspended in a linear shear flow. *J. Fluid Mech.* **113**, 251–267.

BARTHÈS-BIESEL, D., WALTER, J. & SALSAC, A.-V. 2010 Flow-induced deformation of artificial capsules. In *Computational Hydrodynamics of Capsules and Biological Cells*, pp. 35–70. Taylor & Francis.

881 Carin, M., Barthès-Biesel, D., Edwards-Lévy, F., Postel, C. & Andrei, D. 2003 Compression of
882 biocompatible liquid-filled HSA-alginate capsules: determination of the membrane mechanical
883 properties. *Biotechnol. Bioengng.* **82**, 207–212.
884 Cerda, E. & Mahadevan, L. 2003 Geometry and physics of wrinkling. *Phys. Rev. Lett.* **90** (7),
885 074302.
886 Chang, K. S. & Olbricht, W. L. 1993 Experimental studies of the deformation and breakup of a
887 synthetic capsule in steady and unsteady simple shear flow. *J. Fluid Mech.* **250**, 609–633.
888 Cook, R. D., Malkus, D. S., Plesha, M. E. & Witt, R. J. 2001 *Concepts and Applications of Finite*
889 *Element Analysis*, 4th edn. Wiley.
890 Deschamps, J., Kantsler, V. & Steinberg, V. 2009 Phase diagram of single vesicle dynamical states
891 in shear flow. *Phys. Rev. Lett.* **102** (11), 118105.
892 Doddi, S. K. & Bagchi, P. 2008 Lateral migration of a capsule in a plane Poiseuille flow in a
893 channel. *Intl J. Multiphase Flow* **34** (10), 966–986.
894 Dyn, N., Hormann, K., Kim, S.-J. & Levin, D. 2001 Optimizing 3D triangulations using discrete
895 curvature analysis, In *Mathematical Methods for Curves and Surfaces: Oslo 2000*, pp. 135–146.
896 Vanderbilt University.
897 Finken, R., Kessler, S. & Seifert, U. 2010 Micro-capsules in shear flow. *J. Phys.: Condens. Matter*
898 (submitted). **Q1**
899 Finken, R & Seifert, U 2006 Wrinkling of microcapsules in shear flow. *J. Phys.: Condens. Matter*
900 **18** (15), L185–L191.
901 Goldsmith, H. L. & Marlow, J. 1972 Flow behaviour of erythrocytes. Part I. Rotation and
902 deformation in dilute suspensions. *Proc. R. Soc. Lond.* B **182** (1068), 351–384.
903 Hammer, P. C., Marlowe, O. J. & Stroud, A. H. 1956 Numerical integration over simplexes and
904 cones. *Math. Tables Aids Comput.* **10** (55), 130–137.
905 Helfrich, W. 1973 Elastic properties of lipid bilayers: theory and possible experiments. *Z.*
906 *Naturforsch.* (C) **28** (11), 693. **Q2**
907 Jeffery, G. B. 1922 The motion of ellipsoidal particles immersed in a viscous fluid. *Proc. R. Soc.*
908 *Lond.* A **102**, 161–179.
909 Kantsler, V. & Steinberg, V. 2006 Transition to tumbling and two regimes of tumbling motion of
910 a vesicle in shear flow. *Phys. Rev. Lett.* **96** (3), 036001.
911 Keller, S. R. & Skalak, R. 1982 Motion of a tank-treading ellipsoidal particle in a shear flow.
912 *J. Fluid Mech.* **120**, 27–47.
913 Kessler, S., Finken, R. & Seifert, U. 2008 Swinging and tumbling of elastic capsules in shear flow.
914 *J. Fluid Mech.* **605**, 207–226.
915 Lac, É., Barthès-Biesel, D., Pelekasis, N. A. & Tsamopoulos, J. 2004 Spherical capsules in three-
916 dimensional unbounded Stokes flow: effect of the membrane constitutive law and onset of
917 buckling. *J. Fluid Mech.* **516**, 303–334.
918 Le, D.-V. & Tan, Z. 2010 Large deformation of liquid capsules enclosed by thin shells immersed in
919 the fluid. *J. Comput. Phys.* **229** (11), 4097–4116.
920 Lefebvre, Y., Leclerc, E., Barthès-Biesel, D., Walter, J. & Edwards-Levy, F. 2008 Flow
921 of artificial microcapsules in microfluidic channels: A method for determining the elastic
922 properties of the membrane. *Phys. Fluids* **20** (12), 123102.
923 Li, X. & Sarkar, K. 2008 Front tracking simulation of deformation and buckling instability of a
924 liquid capsule enclosed by an elastic membrane. *J. Comput. Phys.* **227** (10), 4998–5018.
925 Liu, L., Yang, J.-P., Ju, X.-J., Xie, R., Yang, L., Liang, B. & Chu, L.-Y. 2009 Microfluidic
926 preparation of monodisperse ethyl cellulose hollow microcapsules with non-toxic solvent.
927 *J. Colloid Interface Sci.* **336** (1), 100–106.
928 Luo, H. & Pozrikidis, C. 2007 Buckling of a pre-compressed or pre-stretched membrane. *Intl J.*
929 *Solids Struct.* **44**, 8074–8085.
930 Oden, J. T. 1972 *Finite Elements of Non-Linear Continua*. McGraw-Hill.
931 Pozrikidis, C. 1992 *Boundary Integral and Singularity Methods for Linearized Viscous Flow*.
932 Cambridge University Press.
933 Ramanujan, S. & Pozrikidis, C. 1998 Deformation of liquid capsules enclosed by elastic membranes
934 in simple shear flow: Large deformations and the effect of capsule viscosity. *J. Fluid Mech.*
935 **361**, 117–143.
936 Risso, F., Collé-Paillot, F. & Zagzoule, M. 2006 Experimental investigation of a bioartificial
937 capsule flowing in a narrow tube. *J. Fluid Mech.* **547**, 149–173.

Schenk, O. & Gärtner, K. 2004 Solving unsymmetric sparse systems of linear equations with PARDISO. *Future Generation Comput. Syst.* **20** (3), 475–487.

Schenk, O. & Gärtner, K. 2006 On fast factorization pivoting methods for sparse symmetric indefinite systems. *Electron. Trans. Numer. Anal.* **23**, 158–179.

Schmid-Schönbein, H. & Wells, R. E. 1969 Fluid drop-like transition of erythrocytes under shear. *Science* **165**, 288–291.

Skalak, R., Tozeren, A., Zarda, R. P. & Chien, S. 1973 Strain energy function of red blood cell membranes. *Biophys. J.* **13**, 245–264.

Skotheim, J. M. & Secomb, T. W. 2007 Red blood cells and other nonspherical capsules in shear flow: Oscillatory dynamics and the tank-treading-to-tumbling transition. *Phys. Rev. Lett.* **98** (7), 078301.

Sui, Y., Low, H. T., Chew, Y. T. & Roy, P. 2008 Tank-treading, swinging, and tumbling of liquid-filled elastic capsules in shear flow. *Phys. Rev.* E **77** (1), 016310.

Walter, A., Rehage, H. & Leonhard, H. 2001 Shear induced deformation of microcapsules: shape oscillations and membrane folding. *Colloids Surf.* A*: Physicochem. Engng. Aspects* **183–185**, 123–132.

Walter, J., Salsac, A.-V., Barthès-Biesel, D. & Le Tallec, P. 2010 Coupling of finite element and boundary integral methods for a capsule in a Stokes flow. *Intl. J. Numer. Meth. Engng.* **83**, 829–850.

Xiang, Z. Y., Lu, Y. C., Zou, Y., Gong, X. C. & Luo, G. S. 2008 Preparation of microcapsules containing ionic liquids with a new solvent extraction system. *React. Funct. Polym.* **68** (8), 1260–1265.